THE SLAC THREE-BODY PARTIAL WAVE ANALYSIS SYSTEM[*]

D. Aston, T.A.Lasinski[a] and P.K. Sinervo

Stanford Linear Accelerator Center
Stanford University, Stanford, California 94305

October 1985

---

[*] Manual.

[a] Present address: NASA, Ames Research Center, Mountain View, CA 94040, USA.

Abstract

We present a heuristic description of the SLAC-LBL three-meson partial wave model, and describe how we have implemented it at SLAC. The discussion details the assumptions of the model and the analysis, and emphasizes the methods we have used to prepare and fit the data.

Table of Contents

List of Tables

List of Figures

1. Introduction

The study of three body final states has been a source of considerable information about excited hadronic states. In particular, the three body decay modes of mesons have given us valuable data on the mass, width, and decay modes of a large number of the excited strange and non-strange states which inhabit the region between 0.5 and 2.0 GeV/c^2.

The three-body isobar model has been used extensively by various experimenters to describe their data on three-body final states. We have employed the SLAC-LBL version of this model in analyses of two previous experiments E-75 and E-132, and are currently using it to analyze the data from a higher statistics experiment E-135. Because of our increasing familiarity with this model, and because of the usual mystery surrounding how it is properly realized in practice, we have prepared this report. It provides a rather informal exposition of the main features of the SLAC-LBL three-body isobar model, and details how we have chosen to implement it at SLAC. Its target audience is the experimenter who is interested in performing a three-body isobar analysis. As such, we have intentionally avoided a rigourous presentation of the model's formalism and have instead focused on how the model is implemented, and what steps are needed to perform the analysis.

As an example, we discuss how we have used this model to analyze our own data, and the software tools that are generally available to make the analysis easier. Of course, our approach to this is not the only possible way to implement the model. However, we feel that it is instuctive to appreciate how we have proceeded if only to avoid some of the pitfalls we have encountered in our studies.

2. The Decay Amplitude

In this chapter we describe in fair detail the form of the three-body decay amplitude. Although we will attempt to discuss all aspects of the amplitude, we will not go into extensive derivations these being done in exhaustive detail elsewhere [1-3].

2.1 THE PROBABILITY DISTRIBUTION

Consider as a model the reaction

$$K_{in}^+ \, p_{in} \rightarrow \pi_i^- \, K_j^+ \, \pi_k^+ \, p_{out} \qquad (2.1)$$

where we cyclically label the three bosons *(ijk)*. We assume that all 4-vectors in (2.1) are known, but that no information on nuclear polarization is available. We write the probability distribution for (2.1) as

$$P = \frac{d^8 s}{d\omega^8} \sum_{\substack{s=+,- \\ \eta=+,-}} \left| \sum A_{s\eta J} X_{\eta J} \right|^2 \qquad (2.2)$$

Equation (2.2) is just the eight fold differential cross section $(12-4=8)$ appropriate to (2.1). Since we assume that nuclear polarization is unmeasured in (2.1), there are four incoherent terms in (2.2) (labeled by s and η described below). One of the eight phase space variables is an azimuthal angle about the beam which may be trivially integrated over. Thus reaction (2.1) may be described by an appropriate choice of seven variables which we shall discuss below.

The $X_{\eta J}$ of (2.2) are the decay amplitudes; they are known functions of the seven variables. The index J denotes a sequence of quantum numbers needed to specify a partial wave ("wave" for short). The index $\eta(=\pm 1)$ is a discrete quantum number ("naturality") which we shall discuss in the next chapter.

The $A_{s\eta J}$ of (2.2) are the complex partial wave amplitudes ("amplitudes") which we want to find from the data by using the probability distribution (2.2) in a likelihood fit. We assume these are only functions of $K\pi\pi$ mass, m, and $p_{in} - p_{out}$ 4-momentum transfer, $t' = t - t_{min}$. In addition to the indices η and J, the amplitudes are also labeled by the net nuclear flip; that is, $s = +$ corresponds

to $+\frac{1}{2} \rightarrow +\frac{1}{2}$ or "non-flip" while $s = -$ corresponds to $+\frac{1}{2} \rightarrow -\frac{1}{2}$ or "flip". For a given η, parity invariance ensures that there are only two independent flip amplitudes. Notice that we associate the same decay amplitude $X_{\eta J}$ with both $A_{+\eta J}$ and $A_{-\eta J}$. This reflects the fact that we have no information on nuclear polarization in (2.1); thus, we do not expect to be able to measure the nuclear flip and non-flip amplitudes. We defer a discussion of the precise meaning of the amplitudes $A_{\pm \eta J}$ to the next section.

2.2 THE MAGIC FORMULA

For ease of discussion, let us write the decay amplitude as

$$X_{\eta J} = C_J \, G_{\eta J} \, B_J. \qquad (2.3)$$

We discuss below each of the factors in (2.3) with the principal aim of establishing notation. In later sub-sections we will more fully discuss the form of $G_{\eta J}$ and B_J.

The factor C_J is simply the product of two Clebsch-Gordan coefficients in isospin space,

$$C_J = C(\tau_i t_i T; \tau_i^z t_i^z T^z) \, C(\tau_j \tau_k t_i; \tau_j^z \tau_k^z t_i^z). \qquad (2.4)$$

This is just the isospin weight of a $K\pi\pi$ final state of isospin T and projection T^z. Notice that there are three independent ways we can get T, T^z:

$$T = \tilde{\tau}_1 + (\tilde{\tau}_2 + \tilde{\tau}_3) = \tilde{\tau}_2 + (\tilde{\tau}_3 + \tilde{\tau}_1) = \tilde{\tau}_3 + (\tilde{\tau}_1 + \tilde{\tau}_2).$$

We refer to these three possibilities as distinct types, or isobars. In other words, for type i we think of bosons jk forming an isospin eigenstate t_i "recoiling" from boson i. Note that for (2.1) the three types are $K_j^+ \pi_k^-$ ($K^{*\prime}s$), $\pi_k^- \pi_i^+$ ($\rho's$), and $\pi_i^+ K_j^+$ ("exotics"). Note also that T, T_z and isobar type are three of the quantum numbers associated with J.

The factor $G_{\eta J}$ in (2.3) is written

$$G_{\eta J} = \begin{bmatrix} \eta = +1 \; Re \\ \eta = -1 \; Im \end{bmatrix} \sqrt{\frac{(2L_i + 1)(2l_i + 1)}{4\pi}}$$

$$\sum_{\lambda_i = -l_i}^{+l_i} C(L_i l_i J; 0\lambda_i \lambda_i) \, D^J_{\lambda_i M}(\alpha_i \beta_i \gamma_i) \, d^{l_i}_{\lambda_i 0}(\theta_i). \qquad (2.5)$$

We will discuss the form of (2.5) in the following subsections. Here it will suffice to define the various quantities in (2.5). From Fig. 1 we see that θ_i is the decay angle of the jk system in its own rest frame, l_i is the spin of the isobar, and m_i is the invariant mass of the isobar. The z-axis is the direction of the recoiling meson π_i^+.
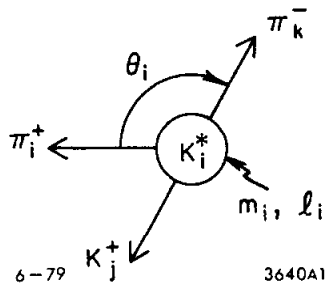
Figure 1. Definition of variables in the K^* isobar rest frame.

To understand the other variables in (2.5), consider the t-channel system sketched in Fig. 2. We associate a coordinate system with this picture as follows. In the $K\pi\pi$ rest system, let the z-axis be in the direction of K_{in}^+. Choose the y-axis normal to the production plane, $\hat{y} = \hat{p}_{in} \wedge \hat{p}_{out}$. For a $K\pi\pi$ system of total spin J, we must have orbital momentum L_i between the π_i^+ and K_i^{*0} (jk isobar, spin l_i): $\vec{J} = \vec{L}_i + \vec{l}_i$. In order to measure the spin of the $K\pi\pi$ system, we must relate the production coordinate system to a decay coordinate system , such as that in Fig. 3. We define the decay coordinate system with the z-axis along the direction of the π^+ and the y-axis normal to the Dalitz plane, $\hat{y} = \hat{K}_j^+ \wedge \hat{\pi}_k^-$. Again, all vectors are in the $K\pi\pi$ rest frame. In terms of these two systems, the remaining angles in (2.5) are

$$
\begin{aligned}
\alpha_i &= \arctan(\frac{\hat{z} \cdot \hat{y}_i}{\hat{z} \cdot \hat{x}_i}); \\
\beta_i &= \arccos(\hat{z} \cdot \hat{z}_i); \\
\gamma_i &= \arctan(\frac{\hat{y} \cdot \hat{z}_i}{\hat{x} \cdot \hat{z}_i}).
\end{aligned}
\tag{2.6}
$$

From Fig. 2 and (2.6) we note that β_i is conjugate to L_i and the magnetic substate of the $K\pi\pi$ system (M=J_z) is conjugate to γ_i.
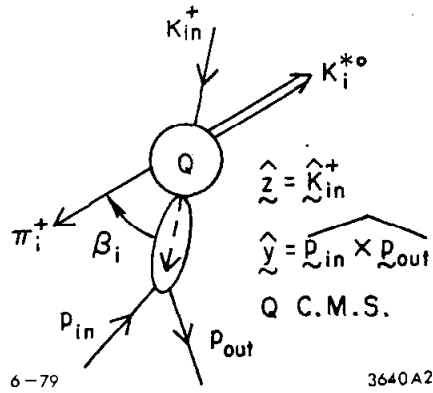
Figure 2. The t-channel production coordinate system.
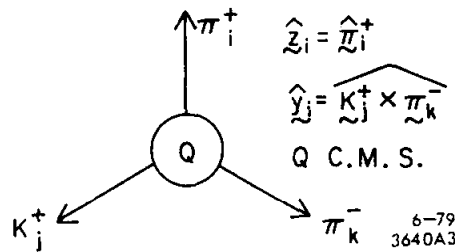
Figure 3. The $K\pi\pi$ decay coordinate system.

Comments:

1. The cyclic notation for specifying types is important! In a case like $\pi^+\pi^+\pi^-$, $X_{\eta J}$ has proper symmetry when the sign changes in both C_J and $G_{\eta J}$ are taken into account.

2. The index J corresponds to the quantum numbers

$$J = \{T, T^z, t_i t_i^z, \tau_i \tau_j \tau_k, \tau_i^z \tau_j^z \tau_k^z; \; JML_i l_i\}. \qquad (2.7)$$

The term "wave" will mean this string of quantum numbers. A more colourful notation which is in general use is

$$\text{Wave} = J^P M^\eta (\text{Isobar}) L. \qquad (2.8)$$

For example the principal wave in the L meson region ($\sim 1750 \; MeV/c^2$) is believed to be the $2^-0^+ K^*(1430)S$.

3. In a final state such as $K^-\pi^-\pi^+ \mathrm{p}$ it is not possible to distinguish $T = \frac{1}{2}$ and $T = \frac{3}{2}$ waves! For example, it is known from comparison with $K^\circ\pi^-\pi^- \mathrm{p}$

that small amounts of $T = \frac{3}{2}$ waves are present. In other final states like $\pi^+\pi^-\pi^\circ$ it is possible to distinguish total isospin states. (Why?)

4. Equations (2.4) and (2.5) are valid for any three-body final state consisting solely of pseudoscalars. A more general expression for arbitrary spins and parities can be found in Ref. 4.

The remaining factor in (2.3), B_J, expresses our *a priori* assumptions about the partial wave amplitude. We shall discuss it further below, but record it here for completeness.

$$B_J = \frac{Q_i^{L_i}}{\sqrt{Q_i^{2L_i} + ... + constant}} f_J(m,t') \frac{e^{i\delta_{l_i}(m_i)} \sin \delta_{l_i}(m_i)}{m \, m_i \, q_i^{l_i+1}}. \qquad (2.9)$$

The first factor in (2.9) is known as the barrier factor. Q_i is the momentum of the isobar of type i and the "bachelor" meson in the three-body CMS.

The second factor $f_J(m, t')$ just emphasizes that other a priori knowledge about a wave could be built in. For example, suppose we knew a given wave J had a momentum transfer behaviour like

$$\exp(b_J(m)t')$$

where the slope b_J was a function of $K\pi\pi$ mass (m). We would model this knowledge in (2.9) with

$$f_J(m,t') = \exp(\frac{b_J(m)t'}{2}).$$

Were this model correct, we would expect $A_{s\eta J}(m,t')$ to be constant for a fixed mass.

The remaining term in (2.9) is the so-called Watson final state interaction factor. q_i is the momentum of particles j and k in the jk rest frame and m_i is the jk invariant mass. The phase shift factor $e^{i\delta}\sin\delta$ (or more generally $(\eta e^{2i\delta} - 1)/2i$) we take from our current knowledge of $\pi\pi$, $K\pi$, KK, etc. scattering for the appropriate isobar.

2.3   DISCUSSION OF THE FORM OF $G_{\eta J}$

At first sight (2.5) seems formidable. Here we elaborate on its structure. To do so, let us consider the decay of a $J^P = 0^-$ particle into a vector meson ($J^P = 1^-$) and a pseudoscalar. The basic quantum mechanical argument goes as follows. First introduce three mutually orthogonal spinors Ψ_{+1}, Ψ_0 and Ψ_{-1} corresponding to the spin projections of the vector meson. With reference to the angles $\Omega \equiv (\Theta, \Phi)$ defined in Fig. 4, the wave function for the 0^- state is then

$$\Psi = \sqrt{\frac{1}{3}} Y_1^{-1}(\Theta, \Phi)\Psi_{+1} - \sqrt{\frac{1}{3}} Y_1^0(\Theta, \Phi)\Psi_0 + \sqrt{\frac{1}{3}} Y_1^{+1}(\Theta, \Phi)\Psi_{-1}.$$

We used the Y_1 spherical harmonics since we need overall spin 0. Note that $|\Psi|^2 = constant$. This is not surprising in view of the fact that the form of Ψ depends intimately on the spin state of the vector meson. Fortunately for our purposes, we can learn about the 1^- projections by letting it decay. We do this by replacing the spinors with spherical harmonics over a second set of angles $\omega \equiv (\theta, \phi)$:

$$\Psi = \sqrt{\frac{1}{3}} Y_1^{-1}(\Theta, \Phi)Y_1^{+1}(\theta, \phi) - \sqrt{\frac{1}{3}} Y_1^0(\Theta, \Phi)Y_1^0(\theta, \phi) + \sqrt{\frac{1}{3}} Y_1^{+1}(\Theta, \Phi)Y_1^{-1}(\theta, \phi).$$

This replacement is justified since the transformation properties in angular momentum theory of the Y_l^M's are the same as for the spinors. Notice that $|\Psi|^2$ is no longer trivial although

$$\int |\Psi|^2 d\omega = constant.$$
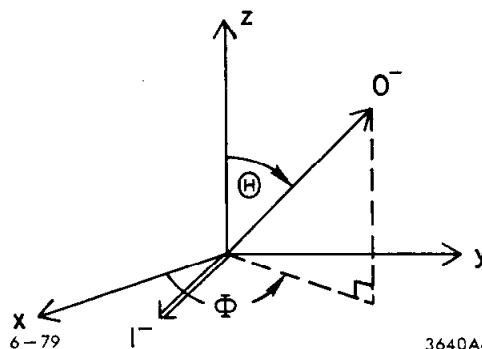
Figure 4. The two body decay coordinate system.

The expression for Ψ is readily generalized:

$$\Psi_{JM} = \sum_{\substack{-L \leq N \leq L \\ -l \leq n \leq l}} C(LlJ; NnM) \, \mathrm{Y}_L^N(\Theta, \Phi) \, \mathrm{Y}_l^n(\theta, \phi), \qquad (2.10)$$

where $JMLl$ have the same meaning as in (2.5). On rather basic grounds, we see that four angles are required to define a spin state for three pseudoscalars.

We next sketch a sequence of formal manipulations which bring (2.10) into the form of (2.5). An alternative discussion can be found in Ref. 5 (section II through equation 2.6). We may think of these angles as specifying rotations in space. Clearly there exists some Euler rotation (specified by the angles τ, χ and ρ) which relates the ω and Ω directions,

$$R(\omega) = R(\Omega)R(\tau\chi\rho),$$

From the properties of the rotation group [6,7], we have

$$D_{n0}^{l*}(\omega) = \sum_\lambda D_{n\lambda}^{l*}(\Omega) D_{\lambda 0}^{l*}(\tau\chi\rho).$$

Since $\mathrm{Y}_L^M(\omega) = \sqrt{\frac{2L+1}{4\pi}} D_{M0}^{L*}(\omega)$, (2.10) becomes

$$\Psi_{JM} = \sum_{\lambda N n} C(LlJ; NnM) \sqrt{\frac{(2L+1)(2\lambda+1)}{16\pi^2}} \, D_{N0}^{L*}(\Omega) \, D_{n\lambda}^{l*}(\Omega) \, D_{\lambda 0}^{l*}(\tau\chi\rho)$$

Now the product of two D functions of the same argument can be reduced via

$$D_{N0}^{L*}(\Omega) \, D_{n\lambda}^{L*}(\Omega) = \sum_{J'M'} C(LlJ'; 0\lambda\lambda) \, C(LlJ'; NnM') \, D_{M'n}^{J'*}(\Omega).$$

Using in addition, the orthogonality property

$$\sum_{Nn} C(LlJ; NnM) \, C(LlJ'; NnM') = \delta_{JJ'} \, \delta_{MM'},$$

we obtain

$$\Psi_{JM} = \sqrt{\frac{(2L+1)(2l+1)}{4\pi}} \sum_\lambda C(LlJ; 0\lambda\lambda) \, D_{M\lambda}^{J*}(\Phi\Theta\tau) \, d_{\lambda 0}^l(\chi). \qquad (2.11)$$

Given that (2.11) can be derived from (2.10), why do we use the perhaps less intuitive form of (2.5)? The answer is simply of historical origin. Equation (2.5) was originally derived for arbitrary spin [4]. The helicity representation was used because keeping track of phases, etc. is easier.

2.4 THE EULER ANGLES $\alpha\beta\gamma$

It is useful to have a physical picture for the angles $\alpha\beta\gamma$. We begin by first discussing the origin of (2.6). We restrict ourselves to one specific isobar type (K^*) in the present discussion.

The rotation $R(\alpha,\beta,\gamma)$ is one which takes the decay or Dalitz coordinates $\hat{x}_D, \hat{y}_D, \hat{z}_D$ (see Fig. 3) into the production coordinates $\hat{x}_p, \hat{y}_p, \hat{z}_p$ (see Fig. 2). To construct this rotation recall [6] that

$$R(\alpha,\beta,\gamma) = \exp(-iJ_z\alpha)\exp(-iJ_y\beta)\exp(-iJ_z\gamma)$$
$$= \exp(-iJ_z''\gamma)\exp(-iJ_y'\beta)\exp(-iJ_z\alpha).$$

Notice that the J_z directions in the second line are different and the order $\alpha\beta\gamma$ has become $\gamma\beta\alpha$.

For the transformation to the production coordinate system, we have:

$$\begin{pmatrix} x_p \\ y_p \\ z_p \end{pmatrix} = \begin{pmatrix} c\gamma & s\gamma & 0 \\ -s\gamma & c\gamma & 0 \\ 0 & 0 & 1 \end{pmatrix} \begin{pmatrix} c\beta & 0 & -s\beta \\ 0 & 1 & 0 \\ s\beta & 0 & c\beta \end{pmatrix} \begin{pmatrix} c\alpha & s\alpha & 0 \\ -s\alpha & c\alpha & 0 \\ 0 & 0 & 1 \end{pmatrix} \begin{pmatrix} x_D \\ y_D \\ z_D \end{pmatrix}$$

$$(2.12)$$

$$= \begin{pmatrix} c\gamma c\beta c\alpha - s\gamma s\alpha & c\gamma c\beta s\alpha + s\alpha c\alpha & -c\gamma s\beta \\ -s\gamma c\beta c\alpha - c\gamma s\alpha & s\gamma c\beta s\alpha + c\gamma c\alpha & s\gamma s\beta \\ s\beta c\alpha & s\beta s\alpha & c\beta \end{pmatrix} \begin{pmatrix} x_D \\ y_D \\ z_D \end{pmatrix}.$$

($c\gamma = \cos\gamma, s\gamma = \sin\gamma$, etc. in 2.12) Equation (2.12) is the well known result for expressing a vector in a new basis in terms of the coordinates in the old basis and the Euler angles which describe the transformation from the old to the new basis. By taking the products

$$\hat{z}_p \cdot \hat{z}_D = \cos\beta$$

$$\hat{x}_p \cdot \hat{y}_D = \sin\beta\sin\alpha$$

$$\hat{x}_p \cdot \hat{z}_D = -\cos\gamma\sin\beta \qquad (2.13)$$

$$\hat{z}_p \cdot \hat{x}_D = \sin\beta\cos\alpha$$

$$\hat{y}_p \cdot \hat{z}_D = \sin\gamma\sin\beta,$$

we readily obtain the result given on (2.6). It is possible to show that $\alpha\beta\gamma$ can be written in terms of Lorentz invariant quantities up to a phase for the azimuthal angles α and γ. For example, one finds (in the notation of Ref. 8) that

$$\sin\alpha = \pm\sqrt{\frac{\Delta_4(p_{K\pi\pi},q_{\pi-},q_{K+},q_{K^+_{in}})\Delta_2(p_{K\pi\pi},q_{\pi+})}{\Delta_3(p_{K\pi\pi},q_{K^+_{in}},q_{\pi-})\Delta_3(p_{K\pi\pi},q_{K^+_{in}},q_{\pi+})}}$$

where the p's and q's are four-vectors and the Δ_n are symmetric Gram determinants.

We can now briefly discuss a physical picture for the angles $\alpha\beta\gamma$. In the production coordinate system, Fig. 5, the π^+ direction may be written

$$\hat{\pi}^+ = \sin\theta\cos\phi\,\hat{x}_p + \sin\theta\sin\phi\,\hat{y}_p + \cos\theta\,\hat{z}_p.$$

However, $\hat{\pi}^+$ is just the orientation of $\hat{z}_D$ in the decay coordinate system. Using (2.13) we thus have

$$\hat{\pi}^+ \cdot \hat{z}_p = \cos\theta = \cos\beta$$

$$\hat{\pi}^+ \cdot \hat{x}_p = \sin\theta\cos\phi = -\cos\gamma\sin\beta$$

$$\hat{\pi}^+ \cdot \hat{y}_p = \sin\theta\sin\phi = \sin\gamma\sin\beta$$

From this we conclude that

$$\theta = \beta \qquad \text{and} \qquad \phi = \pi - \gamma. \qquad (2.14)$$

In words, β and γ are the polar and azimuthal angles of the bachelor meson in the production coordinate system. These angles are more commonly referred to as the Jackson and Treiman-Yang angles. In a similar manner we may write the beam direction as

$$\hat{K}^+_{in} = \sin\theta'\cos\phi'\,\hat{x}_D + \sin\theta'\sin\phi'\,\hat{y}_D + \cos\theta'\,\hat{z}_D.$$
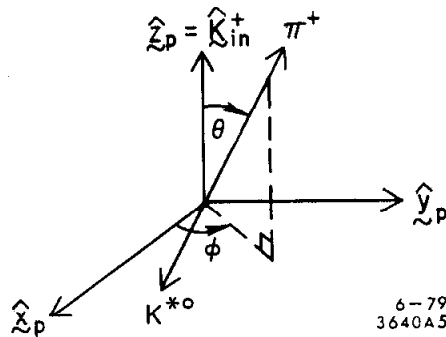
Figure 5. The odd meson (π^+) in the production coordinate system.

From this and (2.13), it follows that β is the polar angle and α is the azimuthal angle of the beam as seen in the decay coordinate system.

2.5   FURTHER REMARKS ON THE FORM OF B_J

The form of the barrier factor in (2.9) has its origin in two body scattering. It is generally accepted [7,9] that

$$\tan \delta_L \overset{Q \to 0}{\sim} aQ^{2L+1}$$

where Q is the center of mass momentum, a is the scattering length and δ_L is the elastic scattering phase shift. This formula is in turn justified by analogy with potential theory or on the basis of general S-matrix theory. To the extent we are studying $K^{*\circ}\pi^+ \to K^{*\circ}\pi^+$ scattering, say, we could write

$$\sigma_L = \frac{4\pi}{Q^2} \left| \frac{\tan \delta_L}{1 - i\tan \delta_L} \right|^2 = 4\pi \left| \frac{aQ^{2L}}{1 - iaQ^{2L+1}} \right|^2 .$$

Thus the elastic amplitude has a threshold behaviour of

$$T \sim Q^{2L}.$$

If the scattering is inelastic, say $K^+\rho^\circ \to K^{*\circ}\pi^+$, this is generalized to

$$T \sim Q_{in}^{L_{in}} Q_{out}^{L_{out}}. \tag{2.15}$$

Since (2.5) and (2.9) represent the decay amplitude, we pick off from (2.15) only the factor of Q_{out}^{Lout}. Note from (2.9) that we have normalized the barrier factor so that it approaches 1 as $Q \to \infty$. This is the ususal practice based more on common sense than any strong physical reason. The explicit forms used for the barrier factors are 10

$$\begin{array}{cc} \sqrt{\dfrac{(QR)^2}{(QR)^2+1}} & \text{for} \quad L=1 \\[4ex] \sqrt{\dfrac{(QR)^4}{(QR)^4+3(QR)^2+9}} & \text{for} \quad L=2, \end{array} \qquad (2.16)$$

where R is set to one fermi.

Phase space for a three-body final state goes as

$$\frac{Q_i}{m}\frac{q_i}{m_i}.$$

One can generalize the arguments concerning (2.15) by guessing that the barrier factor should go as

$$\frac{Q_i^{L_i}}{m}\frac{q_i^{l_i}}{m_i}. \qquad (2.17)$$

The second factor $q_i^{l_i}$ does in fact appear in (2.9) through the Watson factor

$$\frac{e^{i\delta_{l_i}}\sin\delta_{l_i}}{q_i^{l_i+1}}.$$

To see this consider the behaviour of δ_{l_i} where the partial wave is well approximated by a single Breit-Wigner resonance. That is, suppose

$$\tan\delta_{l_i} = \left(\frac{q_i}{q_0}\right)^{2l_i+1}\frac{\Gamma_0/2}{m_0-m_i}$$

where Γ_0 is the width at resonance mass, m_0, and q_i is the K^+ or π^- momentum in the K^{*o} rest system. In this case (2.9) would read

$$B_J = \frac{Q_i^L q^{l_i}}{mm_i}\left[\frac{\Gamma_0/(2q_0^{2l_i+1})}{m_0-m_i-i(\frac{q_i}{q_0})^{2l_i+1}\Gamma_0}\right], \qquad (2.18)$$

2

3. Symmetry Properties, the Observables and the Isobar Model

This section is an extensive discussion of the properties of the amplitudes $A_{s\eta J}(m,t')$ introduced in section 2.2. Symmetry properties include such topics as the number of independent helicity amplitudes and the origin and meaning of the index η. Although we speak in terms of amplitudes, we can measure only density matrix elements averaged over nucleon spin. As will be seen, our amplitudes provide a means through which rank constraints can be imposed on the density matrix. The assumptions of the isobar model are discussed. The existence of the Watson factor, in particular, is crucial to the measurement of the complex off-diagonal matrix elements. Studies of these crucial assumptions are briefly mentioned. To date there is no evidence that these assumptions lead to serious misinterpretations of the data.

3.1 THE DENSITY MATRIX

Equation 1.2 may be written in density matrix form as

$$P = \sum_{s\eta} \left| \sum_{J|M|} A_{s\eta J|M|} X_{\eta J|M|} \right|^2$$

$$= \sum_{\substack{J|M| \\ J'|M'|}} \left(X_{+J|M|} \quad X_{-J|M|} \right) \begin{pmatrix} \sum_s A_{s+J|M|} A^*_{s+J'|M'|} & 0 \\ 0 & \sum_s A_{s-J|M|} A^*_{s-J'|M'|} \end{pmatrix} \begin{pmatrix} X^*_{+J'|M'|} \\ X^*_{-J'|M'|} \end{pmatrix}$$

$$= \sum_{\substack{J|M|\eta \\ J'|M'|}} X_{\eta J|M|} \, \rho^{|M||M'|\eta}_{JJ'} \, X^*_{\eta J'|M'|} \tag{3.1}$$

where

$$\rho^{|M||M'|\eta}_{JJ'} = \sum_s A_{s\eta J|M|} A^*_{s\eta J|M|}. \tag{3.2}$$

In going from (2.2) to (3.1), we have changed notation somewhat and have made explicit the dependence of $A_{s\eta J}$ on $|M|$, the magnitude of J_z in the $K\pi\pi$ system. Notice that the unnormalized density matrix $\rho^{|M||M'|\eta}_{JJ'}$ is block diagonal in η; the sum on s runs over $+,-$, for nucleon non-flip and flip.

In what follows, we discuss the origins of the forms of (3.1) and (3.2). To do so we must backtrack a bit in our derivation of P. In our discussion of the decay

amplitude, no mention was made of the spin nature of the amplitudes. That is, the results of section 2.3 only bring us to the stage where

$$P = \sum_{\substack{\mu=+,- \\ \nu=+,-}} \Big| \sum_{\substack{J \\ -J \leq M \leq J}} \tilde{A}^{JM}_{\mu\nu} \tilde{G}_{JM} C_J B_J \Big|^2$$

$$= \sum_{\substack{J,J' \\ M,M'}} \tilde{G}_{JM} T_J \tilde{\rho}^{MM'}_{JJ'} \tilde{G}^*_{J'M'} T^*_{J'}, \qquad (3.3)$$

where we set $T_J = C_J B_J$ and

$$\tilde{\rho}^{MM'}_{JJ'} = \sum_{\substack{\mu=+,- \\ \nu=+,-}} \tilde{A}^{JM}_{\mu\nu} \tilde{A}^{J'M'*}_{\mu\nu} \qquad (3.4)$$

$$\tilde{G}_{JM} = \sqrt{\frac{(2L+1)(2l+1)}{4\pi}} \sum_{\lambda} C(LlJ; 0\lambda\lambda) D^{J*}_{M\lambda}(\Phi\Theta\tau) d^l_{\lambda 0}(\chi).$$

In (3.4) the summation runs over all four helicity amplitudes $\tilde{A}^{JM}_{++}$, $\tilde{A}^{JM}_{+-}$, $\tilde{A}^{JM}_{-+}$ and $\tilde{A}^{JM}_{--}$.

To bring (3.3) into the final form of (2.1), we must impose the well-known parity constraints for two-particle scattering $a + b \to c + d$ (see, e.g. Ref. 7),

$$f_{\mu_a\mu_b\mu_c\mu_d} = \eta_a\eta_b\eta_c\eta_d(-1)^{\sigma_a-\mu_a+\sigma_b-\mu_b+\sigma_c-\mu_c+\sigma_d-\mu_d} f_{-\mu_a-\mu_b-\mu_c-\mu_d}, \qquad (3.5)$$

where μ denotes helicity, η denotes parity and σ spin. For our purposes (3.5) yields

$$\tilde{A}^{JM}_{\mu\nu} = (-1)^{\mu+\nu+1}(-1)^{J+M+L+l} \tilde{A}^{J-M}_{-\mu-\nu}. \qquad (3.6)$$

In addition, we shall also need the symmetry result

$$\tilde{G}^*_{JM} = (-1)^{J+M+L+l} \tilde{G}_{J-M}. \qquad (3.7)$$

3.2 THE NATURALITY BASIS $|J|M|\eta\rangle$

Define a new set of amplitudes $\mathcal{A}^{\eta J|M|}_{\mu\nu}$, by

$$\mathcal{A}^{\eta J|M|}_{\mu\nu} = N_M(\tilde{A}^{JM}_{\mu\nu} + \eta(-1)^{J+M+L+l} \tilde{A}^{J-M}_{\mu\nu}), \qquad \eta = \pm 1. \qquad (3.8)$$

Here $N_M = \sqrt{\frac{1}{2}}$ for $M \neq 0$ and $N_M = \frac{1}{2}$ for $M = 0$. Note that this new basis $|J|M|\eta\rangle$ spans the same space as $|JM\rangle$. Using (3.6) we have

$$\mathcal{A}_{-\mu-\nu}^{\eta J|M|} = -\eta(-1)^{\mu+\nu}\mathcal{A}_{\mu\nu}^{\eta J|M|}. \tag{3.9}$$

Let us apply this transformation to the sum over JM in (3.3). Using (3.7), (3.8) and taking real and imaginary parts of $\tilde{G}_{JM}$, we have

$$
\begin{aligned}
\sum_{JM} \tilde{A}_{\mu\nu}^{JM} \tilde{G}_{JM} T_J &= \sum_{J|M|} 2N_M^2 \Big\{ \tilde{A}_{\mu\nu}^{JM} \tilde{G}_{JM} + \tilde{A}_{\mu\nu}^{J-M} \tilde{G}_{J-M} \Big\} T_J \\
&= \sum_{J|M|} 2N_M^2 \Big\{ \mathcal{A}_{\mu\nu}^{+J|M|} Re(\tilde{G}_{J|M|}) + i\mathcal{A}_{\mu\nu}^{-J|M|} Im(\tilde{G}_{J|M|}) \Big\} T_J \\
&= \sum_{J|M|\eta} \mathcal{A}_{\mu\nu}^{\eta J|M|} G_{\eta J|M|} T_J
\end{aligned}
\tag{3.10}
$$

where

$$
G_{\eta J|M|} = \begin{cases} Re(\tilde{G}_{JM}), & \eta = +1, \\ Im(\tilde{G}_{JM}), & \eta = -1. \end{cases}
\tag{3.11}
$$

We note here an interesting property for $M = 0$ waves. Since $\tilde{G}_{J0} = (-1)^{J+L+l}\tilde{G}_{J0}^*$ we see that $Im(\tilde{G}_{J0}) = 0$ if $J + L + l$ is even and $Re(\tilde{G}_{J0}) = 0$ if it is odd. From the second line of (3.10), we can conclude that

$$\eta = (-1)^{J+L+l} \qquad \text{for } M = 0. \tag{3.12}$$

We will give a physical picture for this result later.

With the aid of (3.10), the probability distribution (3.3) becomes:

$$
\begin{aligned}
P &= \sum_{\substack{JJ' \\ |M||M'| \\ \eta\eta'}} G_{\eta J|M|} T_J \left(\sum_{\mu\nu} \mathcal{A}_{\mu\nu}^{\eta J|M|} \mathcal{A}_{\mu\nu}^{\eta J'|M'|*} \right) G_{\eta J|M|}^* T_J^* \\
&= \sum_{\substack{JJ' \\ |M||M'| \\ \eta\eta'}} G_{\eta J|M|} T_J \, \rho_{JJ'}^{|M|\eta|M'|\eta'} \, G_{\eta' J'|M'|}^* T_{J'}^*.
\end{aligned}
$$

Using (3.9) we can now see that ρ is block diagonal in η, that is

$$\rho_{JJ'}^{|M|\eta|M'|\eta'} = \delta_{\eta\eta'}\,\rho_{JJ'}^{|M|\eta|M'|\eta'},$$ (3.13)

since, by substitution,

$$\rho_{JJ'}^{|M|\eta|M'|\eta'} = \sum_{\mu\nu} \mathcal{A}_{\mu\nu}^{\eta J|M|}\,\mathcal{A}_{\mu\nu}^{\eta J'|M'|*}$$

$$= \sum_{-\mu-\nu} \mathcal{A}_{-\mu-\nu}^{\eta J|M|}\,\mathcal{A}_{-\mu-\nu}^{\eta J'|M'|*}$$

$$= \eta\eta'\,\rho_{JJ'}^{|M|\eta|M'|\eta'}.$$

If $\eta \neq \eta'$, we see that $\rho_{JJ'}^{|M|\eta|M'|\eta'}$ is equal to the negative of itself and is thus zero. Lastly, we can use (3.9) once again to reduce the number of independent helicity amplitudes,

$$\rho_{JJ'}^{|M||M'|\eta} = \sum_{\nu} \mathcal{A}_{+\nu}^{\eta J|M|}\mathcal{A}_{+\nu}^{\eta J'|M'|*} + \sum_{\mu}\left((-1)\eta(-1)^{-\frac{1}{2}+\mu}\mathcal{A}_{+-\mu}^{\eta J|M|}\right)\left((-1)\eta(-1)^{-\frac{1}{2}+\mu}\mathcal{A}_{+-\mu}^{\eta J'|M'|*}\right)$$

$$= 2\sum_{\nu} \mathcal{A}_{+\nu}^{\eta J|M|}\mathcal{A}_{+\nu}^{\eta J'|M'|*},$$ (3.14)

since the sum over ν is complete. Using (3.13) and (3.14) we finally obtain

$$P = \sum_{\eta\nu}\left|\sum_{J|M|}\sqrt{2}\mathcal{A}_{+\nu}^{\eta J|M|}\,G_{\eta J|M|}\,C_J\,B_J\right|^2,$$

which is essentially the form of (2.2). We can now make the identification

$$A_{+\eta J} = \mathcal{A}_{++}^{\eta J|M|} \quad \text{and} \quad A_{-\eta J} = \mathcal{A}_{+-}^{\eta J|M|}$$

between the partial wave amplitudes $A_{s\eta J}$ and the helicity amplitudes.

3.3 FURTHER REMARKS ON η

The transformation to the $|J|M|\eta\rangle$ basis is well known in the literature. Technically η indexes what are called parity eigenstates. That is, if Π_{y_p} denotes the reflection operator in the production plane (cf. Fig. 2), then

$$\Pi_{y_p}|J|M|\eta\rangle = -\eta|J|M|\eta\rangle.$$

A succinct discussion of this symmetry is given in the beginning of section II of Ref. 11. Note that from the point of view of the partial wave formulation, the meaning of η is exact and well defined as indicated by the above formal algebra.

A more colourful nomenclature for η is naturality. This stems from the fact that η may be identified with the parity and spin of the system exchanged to produce the $K\pi\pi$ system:

$$\eta = P_{ex}(-1)^{J_{ex}} \tag{3.15}.$$

For $M = 0$, (3.15) follows from a simple argument in the rest system of the exchanged particle (see Fig. 6). If L_{ex} is the orbital momentum between the K_{in}^+ and the $K\pi\pi$ system, then

$$\vec{J}_{ex} = \vec{J} + \vec{L}_{ex}$$
$$P_{ex} = (-1)P(-1)^{L_{ex}}.$$

For $\vec{J}$ and $\vec{L}_{ex}$ to couple to yield $\vec{J}_{ex}$ requires that $C(L_{ex}, J, J_{ex}; 0, 0, 0)$ to be non-zero. This is true only if $L_{ex} + J + J_{ex}$ is even, that is

$$(-1)^{L_{ex}+J+J_{ex}} = 1$$

or

$$(-1)^J = (-1)^{L_{ex}+J_{ex}}.$$

Recalling (3.12) and using $P = -(-1)^{L+l}$, we have

$$P_{ex}(-1)^{J_{ex}} = -P(-1)^J = (-1)^{J+L+l} = \eta.$$

For $M \neq 0$, the assertion that the linear combination of helicity amplitudes given by (3.8) isolates naturality (3.15) is valid only to order $(1/s)$ [7,12].
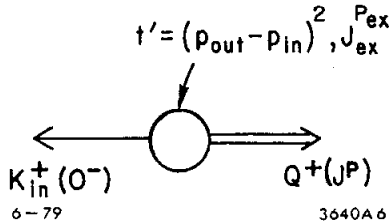
Figure 6. The rest system of the exchanged particle.

The above physical picture for η is often useful in guessing which of the four incoherent terms in (2.2) a particular partial wave is most likely to contribute to. We give two examples of this sort of reasoning for the $K^*(1430)$ wave, the $2^+ M^\eta K^* D$. Consider first the reaction $K^- p \to \bar{K}^\circ \pi^+ \pi^- n$. What value of M^η might we expect? As this is a charge exchange process, we might guess that π-exchange is important. Thus $\eta = -1$. Then given the rule (3.12), we would certainly include the $2^+ 0^- K^* D$ wave in our fit. Furthermore, since π's prefer to couple to proton-neutron flip amplitudes, we would single out the corresponding flip amplitude for the $2^+ 0^- K^* D$ as most important. For our other example consider the diffractive reaction $K^- p \to K^- \pi^+ \pi^- p$. Diffraction brings to mind Pomeron exchange and nucleon non-flip. Again appealing to (3.12), we would guess the non-flip $2^+ 1^+ K^* D$ wave to be the most important.

3.4   THE OBSERVABLES IN THE ANALYSIS

Having established the formalism and notation, we are now in a position to discuss what it is we can measure in the partial wave analysis. It cannot be emphasized too strongly that we are *not* measuring helicity amplitudes and their phases. Indeed we are *not even* measuring relative phases between these amplitudes.

We begin by recording those quantities which are presented as the results of a partial wave analysis.

$$\frac{d^2\sigma}{dm\,dt'} = \frac{\sigma_0}{\Delta m \Delta t'} \sum_s \left[|A_{s\eta J}|^2 \frac{\int |X_{\eta J}|^2 d\omega^5}{\int d\omega^5} \right], \qquad (3.16)$$

where σ_0 is the microbarn equivalent for a fit in an m, t' bin of area $\Delta m \Delta t'$. As discussed later, the likelihood fit is normalized such that (3.16) without the factor of $\sigma_0/\Delta m \Delta t'$ is just the number of produced events in the m, t' bin. The integrals in (3.16) are integrated over the angles α, β, γ and the Dalitz plot variables m_i, θ_i of the particular isobar specified by J; this factor is included to restore the m, t' effects of B_J to the cross section.

The isobar model permits us to measure both the real and imaginary parts of the off-diagonal elements of the density matrix. Such measurements are traditionally expressed in terms of a relative phase and coherence between two "waves". The

relative phase between two waves I and J is given by

$$\phi_{IJ\eta} = arg\left(\sum_s A_{s\eta I} A_{s\eta J}{}^*\right),\qquad(3.17)$$

where both waves can only have the same η. The coherence is defined by

$$C_{IJ\eta} = \frac{\left|\sum_s A_{s\eta I} A_{s\eta J}{}^*\right|}{\sqrt{\left[\sum_t |A_{t\eta I}|^2\right]\left[\sum_u |A_{u\eta J}|^2\right]}}.\qquad(3.18)$$

If $C_{IJ\eta}$ happens to be equal to one, it is easily seen that we may interpret $\phi_{IJ\eta}$ as the phase between two waves *with the same helicity*. Such an interpretation, however, is not unique as we shall see in the discussion of coherence in the next section. Furthermore, $C_{IJ\eta}$ is often less than one in practice. In such cases some care must be taken in interpreting $\phi_{IJ\eta}$ as the phase between two partial wave amplitudes.

The last observable is known as the interference term between two waves of the same $J^P M^\eta$ but with different isobars. It is defined by

$$\left(\frac{d^2\sigma}{dmdt'}\right)_{IJ\eta} = 2\frac{\sigma_0}{\Delta m\Delta t'}Re\left(\sum_s A_{s\eta I} A_{s\eta J}{}^*\frac{\int X_{\eta I} X_{\eta J}{}^* d\omega^5}{\int d\omega^5}\right),\qquad(3.19)$$

where the notation is similar to that of (3.16). It should be emphasized that (3.19) exists only for waves of the same $J^P M^\eta$. Although the integral in (3.19) extends over the Dalitz plot, the interference term has a more basic origin than the overlap of two isobars. In particular, one may show [2,13]

$$\int G_{J^P M^\eta}(\alpha,\beta,\gamma)\, G_{J'^{P'} M'^\eta}(\alpha,\beta,\gamma)\, d\alpha\, d(\cos\beta)\, d\gamma$$

$$= \delta_{JJ'}\, \delta_{MM'}\, \delta_{PP'}\, f_J(m,t').$$

This is a technical statement of two fairly obvious facts. First, it is well known that states of different $J^P M^\eta$ cannot interfere across the Dalitz plot. Secondly, we observe that $G_{\eta J}$ for a given type, say K^*, form a complete set; the angular

structure of the $K\pi\pi$ system can be represented by using only partial waves of the K^* type. In using the isobar model, we are mixing two types, e.g. K^* and ρ. It is evident that each wave of the K^* type must contain some contribution from a ρ type since both representations are complete. This overlap, in turn, must be across the Dalitz plot for a given $J^P M^\eta$. The practical consequence of this discussion is that the total number of observed events for a given $J^P M^\eta$ will not be $\sigma_I + \sigma_J$, but rather $\sigma_I + \sigma_J + \sigma_{IJ}$.

As noted at the outset, it is meaningless to interpret the amplitudes $A_{\pm\eta J}$ as helicity amplitudes since we have no polarization information for reaction (2.1). Note that in our definition of observables above, we always summed over s. We now show that while we can measure, for the most part, the $A_{s\eta J}$ complex numbers, we can only base physical conclusions on the observables (3.16–3.19). Consider the arbitrary transformation in helicity space,

$$A_{s\eta J|M|} = \sum_{s'} U_{ss'} B_{s'\eta J|M|} \qquad (3.20)$$

where U is an arbitrary unitary matrix ($U^\dagger U = UU^\dagger = \mathbf{1}$) and $B_{s\eta J|M|}$ are a new set of amplitudes. Notice that we use only one U for all waves. It is easily seen (do it!) that (3.20) leaves all observables unchanged for all waves,

$$\rho_{JJ'}^{|M||M'|\eta} = \sum_s A_{s\eta J|M|} A_{s\eta J'|M'|}^*$$
$$= \sum_s B_{s\eta J|M|} B_{s\eta J'|M'|}^*. \qquad (3.21)$$

Equations (3.20) and (3.21) are just the mathematics of saying we have no information on nucleon polarization — the orientation in "spin-space" is undefined.

Even though we can't identify the $A_{s\eta J}$ with the "true" helicity amplitudes, it is easy to see that we can still measure these amplitudes. Consider P for a given η,

$$P = \left| \sum_J A_{+\eta J} X_{\eta J} \right|^2 + \left| \sum_J A_{-\eta J} X_{\eta J} \right|^2. \qquad (3.22)$$

Suppose there are N_w waves present, and that each wave corresponds to a different isobar or Watson factor. Notice that for a given η, the $G_{\eta J}$ are relatively

real so that it is the complex factor $e^{i\delta} \sin \delta$ that permits us to measure $Re\left(A_{s\eta J}\right)$ and $Im\left(A_{s\eta J}\right)$.

In the first term of (3.22) there are $2N_w - 1$ real numbers to be measured since there are N_w amplitudes and one overall arbitrary phase. It is fairly evident that the first term of (3.22) possesses sufficient information through the direct $\left(\left|X_{\eta J}\right|^2\right)$ and cross $\left(X_{\eta J} X_{\eta I}^*\right)$ terms to measure these $2N_w - 1$ parameters.

Let us turn to the second term in (3.22). Its formal structure is identical to the first term. In particular, were there also N_w waves present in it, it is evident that any fitting scheme would be unable to distinguish these two terms, the decay amplitude $X_{\eta J}$ being the same. Suppose we drop one wave from the second term. In this case, there would be $2N_w - 3$ parameters in the second term. Since the interference patterns of the two terms in (3.22) are now different, it seems plausible that $4N_w - 4$ parameters can be measured. This conclusion is discussed more carefully in Ref. 11. Notice the same reasoning will apply to both $\eta = \pm$ contributions to P.

We conclude this section with a collection of random remarks.

Remark 1 : Amplitudes versus density matrices.

The correct interpretation of our amplitudes is that they provide a means of imposing rank constraints on the density matrix. Recall (3.1),

$$P = \sum_{IJ\eta} X_{\eta I} \, \rho_{IJ\eta} \, X_{\eta J}^* \qquad (3.1')$$

where we have condensed the notation again so that I, J run over all the wave labels. It is perfectly feasible in principle to fit the data using (3.1') and the $\rho_{IJ\eta}$ as free parameters. This, in fact, is the approach taken by Ascoli and colleagues. Studying P in terms of amplitudes tells us, however, that the rank of $\rho_{IJ\eta}$ must in principle be four (two for each η); that is, $\rho_{IJ\eta}$ can have only four non-zero eigenvalues. The rank four condition can be ensured in the density matrix approach provided

$$\left|\rho_{IJ\eta}\right|^2 \leq \rho_{II\eta} \, \rho_{JJ\eta}$$

for all waves.

<u>Remark 2</u> : Why then $\rho_{IJ\eta}$?

The Ascoli approach chooses not to impose the rank four condition. There are two motivations for not doing so. In any real experiment there are effects which could artificially introduce incoherence and thus increase the rank of $\rho_{IJ\eta}$. These effects are

1. "broad" binning of the data in either m or t', and

2. finite resolution of the measurements of the final state.

Examples of how these concerns can affect a partial wave analysis are given by Cashmore [14] and Chaloupka [15].

The other reason for using $\rho_{IJ\eta}$ relates to the non-orthogonality of the $X_{\eta J}$ (Recall (3.19) and the associated discussion). The use of the isobar model makes the concept of a density matrix and rank conditions somewhat questionable when all the basis functions are not properly orthogonal.

<u>Remark 3</u> : Why then $A_{s\eta J}$?

With increasing $K\pi\pi$ mass the number of partial waves N_w which we can measure increases. For the $\rho_{IJ\eta}$ approach, the number of free parameters is growing like N_w^2 while for the $A_{s\eta J}$ approach, like $4N_w$. This additional fact of life indeed forces the Ascoli approach to introduce plausible assumptions to reduce the number of parameters (see Ref. 3 or Ref. 1).

Unfortunately, these assumptions are not always justified to the extent that they could cause more problems than the concerns of Remark 2. In particular, Hansen did not observe the s-channel helicity nature of the $1^+K\rho$ waves until they were disregarded [16].

The amplitude approach solves the parameter density problem with minimal (and, in principle, no) assumptions. The concern over incoherence effects due to broad binning is best handled by doing high statistics experiments. Although better measurement techniques can ameliorate the concern about resolution, it will always be with us. In particular, while we can write down likelihood functions which model resolution, their non-linear nature precludes analysis in a reasonably finite amount of time. The rank condition imposed by the amplitude approach is not *a priori* justified given the non-orthogonality of the basis functions across the Dalitz plot. It is, however, correct in the limit of narrow isobars or zero overlap. The effects

due to the isobar model are at least well defined in the amplitude approach.

Remark 4 : Ambiguities

Consider (3.22) in the situation where all waves have the same isobar. The Watson factor, $e^{i\delta} \sin \delta$, being common to all waves would contribute no phase information in (3.22). Since the $G_{\eta J}$ are relatively real, we could no longer measure $\phi_{IJ\eta}$ but only $\cos \phi_{IJ\eta}$. This is precisely the situation in $K\pi$ scattering studied in reactions such as $K^- p \to K^- \pi^+ n$. In this limit we must recover the well known ambiguities of $K\pi$ or $\pi\pi$ scattering.

3.5 SOME COMMENTS ON COHERENCE

We elaborate here on the meaning of the coherence observable (3.18). We restrict the discussion to waves of the same η since the density matrix is block diagonal in η. As noted above, the use of amplitudes ensures that the density matrix can only have two non-zero eigenvalues for each η. These non-zero eigenvalues are given by

$$\lambda = \frac{1}{2} \sum_I \rho_{II\eta} \pm \frac{1}{2} \sqrt{\left(\sum_I \rho_{II\eta} \right)^2 + 4 \sum_{I \neq J} \left(|\rho_{IJ\eta}|^2 - \rho_{II\eta} \rho_{JJ\eta} \right)}. \qquad (3.23)$$

Notice the connection between the second term under the radical sign and the definition of coherence in (3.18). In particular, there are two interesting limiting cases governed by the value of $C_{IJ\eta}$. If $C_{IJ\eta} = 1$ for all waves, then

$$\lambda = \begin{cases} \rho_{II\eta} \\ 0 \end{cases} \qquad C_{IJ\eta} = 1. \qquad (3.24)$$

We call this case perfect coherence; there is only one non-zero eigenvalue given by the sum of the diagonal elements of $\rho_{IJ\eta}$. In the other extreme, suppose $C_{IJ\eta} = 0$ for all waves. Then we have

$$\lambda = \begin{cases} \rho_{II\eta} \\ \sum_{I \neq J} \rho_{IJ\eta} \end{cases} \qquad C_{IJ\eta} = 0. \qquad (3.25)$$

We refer to this case as perfect incoherence; notice the distinct role played by some wave J in (3.25) (recall the discussion following (3.22)).

To gain some insight into the meaning of coherence, we next consider a model consisting of only two waves. Denoting nucleon helicity non-flip and flip amplitudes by n_i and f_i respectively, the density matrix elements may be written as

$$\rho_{11} = |n_1|^2 + |f_1|^2$$
$$\rho_{21}^* = \rho_{12} = n_1 n_2^* + f_1 f_2^* \tag{3.26}$$
$$\rho_{22} = |n_2|^2 + |f_2|^2.$$

If we think of the pair (n_i, f_i) as being a vector in "spin space", then the density matrix elements of (3.26) are all the possible complex dot products of the vectors (n_1, f_1) and (n_2, f_2). By Schwartz's inequality, we see that the coherence is bounded,

$$0 \leq C_{12} = \frac{|\rho_{12}|}{\sqrt{\rho_{11}\rho_{22}}} \leq 1. \tag{3.27}$$

Consider the upper limit of (3.27), $C_{12} = 1$. From (3.26) this implies

$$|n_1 f_2 - n_2 f_1| = 0. \tag{3.28}$$

There are two interpretations of this limit.

1. Both f_1 and f_2 zero. Physically we would say that both waves are produced solely by nucleon helicity non-flip.

2. $n_1/f_1 = n_2/f_2$. This says the vectors in spin space are parallel, as shown in Fig. 7.In this sense we may think of (3.28) as requiring the cross-product of the two spin vectors to equal zero, implying that the vectors must be parallel or anti-parallel.

As noted in (3.24), perfect coherence leads to the eigenvalues $\lambda = \rho_{11} + \rho_{22}$ and $\lambda = 0$.

The lower limit of (3.27), $C_{J J_\eta} = 0$, has a similar interpretation. Since

$$|\rho_{12}| = |n_1 n_2^* + f_1 f_2^*| = 0$$

we say the spin vectors are orthogonal. The simplest physical interpretation is to say that one wave is produced via helicity non-flip while the other by helicity flip.
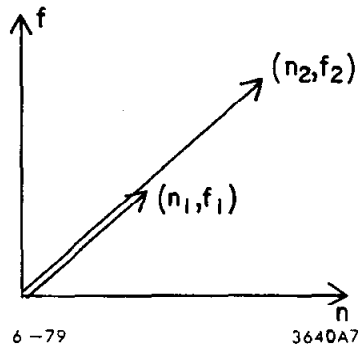
Figure 7. Perfect Coherence of an Amplitude. The most general orientation of the flip and non-flip amplitudes of a perfectly coherent wave.

Clearly, this viewpoint is not unique. The eigenvalues of the density matrix for perfect incoherence are $\lambda = \rho_{11}$ and $\lambda = \rho_{22}$.

We conclude our remarks on coherence by considering two effects which most likely do not reflect the behaviour of actual helicity amplitudes. They are most likely induced coherence effects[14,15]due to particular experimental procedures. In Fig. 8 we show measured coherence as a function of t' in the $K\pi\pi$ mass interval $1.2 - 1.35 \ GeV/c^2$. The results are two coherence parameters, $C_{(1^+0^+\rho S, \, 1^+0^+ K^* S)}$ and $C_{(1^+1^+\rho S, \, 1^+0^+ K^* S)}$, from two $K^- p \rightarrow K^- \pi^+ \pi^- p$ experiments performed at comparable energies, and labeled SLAC (E75) and B.C. [17].Other results (intensities, phases, etc.) from these two experiments are known to be consistent. While these coherences agree at "large" t', they show strikingly different systematic behaviour as $t' \rightarrow 0$. The B.C. results suggest that the coherence for these waves vanishes as $t' \rightarrow 0$. A possible physical interpretation of such a result is that the $1^+\rho$ system corresponds to a pure helicity flip amplitude while the $1^+0^+K^*S$ wave is produced with some combination of flip and non-flip amplitudes. The SLAC results, in contrast, suggest a value closer to one as $t' \rightarrow 0$; note carefully, however, that the systematic trend is to a finite value less than one. Since the SLAC results are close to one for all t', one might argue that both the $1+\rho$ and 1^+K^* systems are produced with pure helicity non-flip amplitudes, characteristic of diffractive production.

It may be shown in general that coherence must approach either zero or one as $t' \rightarrow 0$. We now argue that the spurious SLAC results are most likely incoherent effects generated by averaging over a broad mass bin. The amplitudes we are
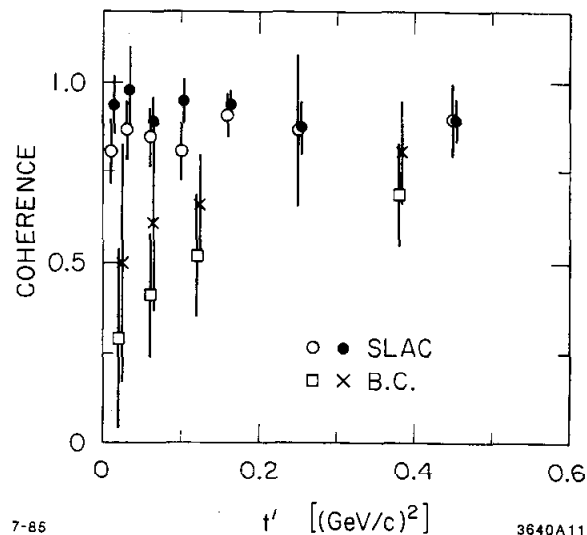
Figure 8. Coherence as a function of t'. Comparison of results from two experiments studying $K^-p \rightarrow K^-\pi^+\pi^-p$. The open and closed circles show the coherence of the $1^+0^+\rho S$ and the $1^+1^+\rho S$ waves determined from the SLAC data. The squares and ×'s are the corresponding results from the B.C. data.

measuring are functions of both m and t',

$$A(m,t') = \left|A(m,t')\right| e^{i\phi(m,t')} \cong \left|A(m)\right| e^{i\delta} \left|b(t')\right| e^{i\alpha(t')}. \qquad (3.29)$$

We often think of $A(m,t')$ as though we can factor the m, t' dependence as indicated by the approximate equality in (3.29). If the wave is resonant we would expect A to show a Breit-Wigner phase behaviour. Based on Regge theory we might expect $\alpha(t')$ to vary slowly. If the wave is helicity flip, we would expect $\left|b(t')\right|$ to vary rapidly

as $\sqrt{-t'}$. With (3.29) in mind we can make a crude estimate of how much the coherence might be distorted if we average over a broad mass bin, $1.22 \leq m \leq 1.34$ GeV/c for the SLAC data. Thus

$$\rho_{12} \sim \int |n_1||n_2| \exp(i\phi_1\phi_2) \, dm$$

$$\sim |n_1||n_2| \left(\langle \cos \phi_{rel} \rangle + i \langle \sin \phi_{rel} \rangle \right),$$

where ϕ_{rel} is the measured relative phase and $\langle \cdots \rangle$ denotes a mass average. This suggests a distortion in observed coherence by

$$\frac{C_{obs}}{C_{true}} \sim |\langle \cos \phi_{rel} \rangle + i \langle \sin \phi_{rel} \rangle| \equiv r. \qquad (3.30)$$

In the limit of a small mass bin or where ϕ_{rel} changes slowly with mass, the ratio becomes one. However, in this case the relative phases of these waves are varying substantially with m; in addition, the $1^+\rho$ intensity shows a Breit-Wigner behaviour across the mass interval. Indeed averaging $\cos \phi_{rel}$ and $\sin \phi_{rel}$, we estimate that $r = .95$; that is, an observed coherence is only 95 % of the true coherence due to mass averaging effects.

Turning to the B.C. results of Fig. 8, we indicate reasons why $C \to 0$ as $t' \to 0$ is unlikely. As $t' \to 0$, the K^- and π^- will, in an average sense, be faster in the lab. In a bubble chamber, fast K's and π's are less likely to be distinguishable by ionization. The B.C. experiment was forced to ignore such ambiguous events in the partial wave analysis. Since these events are intuitively correlated with low t', there exists a possibility that dropping them from the analysis led to the vanishing coherence at low t'.

3.6   ASSUMPTIONS OF THE ISOBAR MODEL

"It's well known that the

isobar model is wrong.

...but it gets the right results!"

Cashmore, 1976

With due deference to the pragmatic wisdom of the above quotation [18],we now discuss the crucial approximations of the isobar model. Our remarks will be

necessarily qualitative and sketchy. Detailed and quantitative results may be found in the references; the talk by Aitchison [19] remains a fine introduction.

We begin by restricting ourselves to two waves with the same $J^P M^\eta$ but of different type, K^* and ρ. The wave function for the state is then

$$A_{K^*}(m, m_{K^*}, t') \, B_{K^*} \, G_{K^*} + A_\rho(m, m_\rho, t') \, B_\rho \, G_\rho. \qquad (3.31)$$

Here B_{K^*} and B_ρ denote the Watson factors, and G_{K^*} and G_ρ are the decay amplitudes of (2.5). Barrier factors and Clebsch-Gordan coefficients have been absorbed into the amplitudes A_{K^*} and A_ρ; they and the t' dependence are essentially irrelevant for our discussion. Note, however, that these amplitudes are now functions of the sub-energies m_{K^*} and m_ρ. The principal assumption of the isobar model is that

$$A_{K^*}(m, m_{K^*}, t') \simeq A_{K^*}(m, t')$$
$$A_\rho(m, m_\rho, t') \simeq A_\rho(m, t') \qquad (3.32)$$

that is, the amplitudes are only *weakly* dependent on sub-energy. As discussed in §3.4, G_{K^*} and G_ρ are **not** orthogonal across the Dalitz plot; we are mixing complete representations of the $K\pi\pi$ system. The second assumption of the isobar model is roughly stated as

$$\int B_\rho \, G_\rho \, B_{K^*}^* \, G_{K^*}^* \, d\omega^5 \simeq 0 \qquad (3.33)$$

that is, the overlap between different representations with Watson factors included is small. In the limit of narrow isobars, (3.33) becomes clearly valid and (3.32) would also hold.

In principle the amplitudes A are always a function of sub-energy simply by the nature of angular momentum representations for three-body states; if we carefully (see, e.g. Ref. 20) record all the labels for our basis vectors we get

$$|J^P M^\eta L\, l; \, m\, m_i\rangle.$$

There is a more physical way to appreciate that the amplitudes must be functions of two-body mass. Consider a situation where an isobar partial wave (i.e. $e^{i\delta} \sin \delta$)

resonates twice. For example, the favoured $I = 1$ P-wave amplitude in $\pi\pi$ scattering shows resonance behaviour both at the ρ mass of $\sim 770 \ MeV/c^2$ and again in the vicinity of $\sim 1600 \ MeV/c^2$, which has been taken as evidence for the $\rho'(1600)$; a similar situation exists in the $I = \frac{1}{2}$ P-wave Kπ scattering. We may think of the three-body state as having decay modes into both the $\rho(772)K$ and $\rho'(1600)K$ isobar states. In this situation, however, all the quantum numbers $J^P M^\eta L l$ are the same for both modes; only through the $\pi\pi$ mass dependence can we distinguish which mode is more important. For a given three-body mass, we could in principle measure the relative decay rates by introducing two amplitudes A_ρ and $A_{\rho'}$ and by splitting the Watson factor into two pieces

$$\left(A_\rho B_\rho + A_{\rho'} B_{\rho'} \right) G_\rho \tag{3.34}$$

where we would take

$$B_\rho = \begin{cases} e^{i\delta_\rho} \sin \delta_\rho, & m_{\pi\pi} < 1 \ GeV/c^2; \\ 0, & m_{\pi\pi} \geq 1 \ GeV/c^2. \end{cases}$$

$$\tag{3.35}$$

$$B_{\rho'} = \begin{cases} 0, & m_{\pi\pi} < 1 \ GeV/c^2; \\ e^{i\delta_{\rho'}} \sin \delta_{\rho'}, & m_{\pi\pi} \geq 1 \ GeV/c^2. \end{cases}$$

Although the definitions of ρ and ρ' made by (3.35) are somewhat arbitrary, it is evident that such a procedure would permit us to measure the two amplitudes A_ρ and $A_{\rho'}$.

The above example clearly illustrates potential pitfalls in assuming (3.32). We might hope that for narrow isobars this assumption is not too bad. Unfortunately, taking K^* and ρ as typical "narrow" isobars and (3.33) as a measure of how much they overlap, we still find reason for concern. We show in Fig. 9 the overlap (3.19) for the $1^+ 0^+ \rho S$ and $1^+ 0^+ K^* S$ waves. The data are from the E75 $K^+ \pi^+ \pi^- p$ analysis. The correlation between direct and interference terms, Fig. 9(a), is quite similar to the relative phase behaviour between these waves. From Fig. 9(b) we see that the interference is at least 20 % of the $1^+ 0^+ \rho S$ intensity at peak. We must conclude that assumption (3.33) is, in practice, not true. Furthermore, there is a concern that the measurements we interpret as indicative of resonances are somewhat spurious effects due to using (3.31) with the assumption of (3.32).
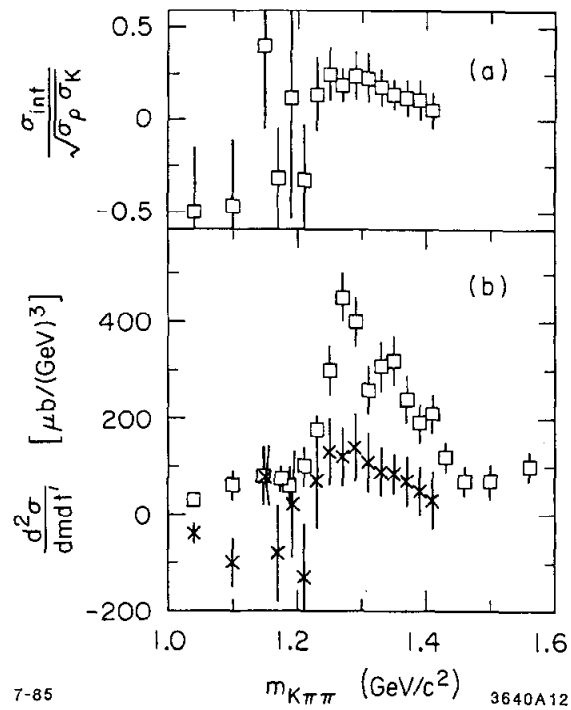
Figure 9. Interference of the $1^+0^+\rho S$ and $1^+0^+K^*S$ waves. Shown is the ratio of the interference term to the direct terms for the $1^+0^+\rho S$ and $1^+0^+K^*S$ waves as a function of $K\pi\pi$ mass (a), and the absolute intensities of the $1^+0^+\rho S$ wave (square's) and the interference term ($\times$'s) (b).

From a theoretical point of view, a formulation of the isobar model using (3.31) and (3.32) is immediately at odds with a subset of unitary constraints. Schematically these are written

$$\text{(3.36)}$$

Here we are considering a 2 → 3 process; the 2 → 3 bubble represents this amplitude while the 2 → 2 bubble refers to the isobar amplitude (i.e. the Watson factor). The ± signs refer to whether we approach the real axis from above or below the cut in isobar mass. In principle (3.36) should hold for all isobar types. If we had only one isobar type, (3.36) would be easily satisfied, viz

$$A(m)e^{i\delta}\sin\delta - A(m)e^{-i\delta}\sin\delta = 2iA(m)e^{i\delta}\sin\delta e^{-i\delta}\sin\delta$$
$$A(m)\left[\frac{e^{i\delta} - e^{-i\delta}}{2i}\right]\sin\delta = A(m)\sin^2\delta.$$

However, as soon as we have two types, (3.36) no longer holds. In particular we are again forced into concluding that the A's must be functions of two-body mass in a manner governed by the strength of the overlap (3.33).

It is possible [21,22] to reformulate the isobar model so that it satisfies the sub-energy unitarity constraints (3.36). Ascoli [21] used such a model to fit 3π data and compared the results from the more traditional approach. There were two interesting results from this study. First it was found that no major qualitative features of the fits were changed, such as intensities or phases. While large changes in various details occurred, no evidence of the hoped-for phase variation signaling an A_1 resonance state was found. The second observation was that the quality of the fits was significantly worse. Although it may be argued that the likelihoods of different models are not directly comparable, it is disconcerting that the supposedly "improved" unitary formulation led to a poorer description of the data.

Shortly after the introduction of the unitarized isobar model, Aitchison [19] observed that such a formulation was still in principle incomplete. In particular he argued that a formulation based solely on unitarity only imposed constraints on the imaginary part of the ampltitude. Schematically,

$$Im(T) = \sum_{isobars} |T|^2.$$

A proper formulation should use this result and a dispersion relation (i.e. analyticity of the scattering amplitude) to put constraints on the real part of the amplitude. In addition, Aitchison also noted that K-matrix approaches, which are equivalent to only constraining $Im(T)$, were well known to often cause "violent" changes in the amplitude. In this sense he was not surprised that the unitarized formulation was less consistent with the data.

The criticisms voiced by Aitchison have been addressed by Schult and Wyld [23]. As emphasized by Schult and Wyld, their particular implementation of analyticity is not unique but is most likely representative of what would arise in a more complete theory. Using a now analytic, unitary formulation of the isobar model, they fit the same data studied by Ascoli and Wyld [21]. When they compared their results with the results from the basic model incorporating the assumptions of (3.31) and (3.32), they found no significant difference in phases or intensities. Furthermore, the description of the data provided by the new model was just as good as that of the basic formulation.

Given the theoretical complexities of the problem, it is dangerous to draw strong conclusions from these encouraging results of Schult and Wyld. We shall, however, offer the following guidelines[24] for results obtained with the isobar model. Measurements of comparatively large phase changes or intensities as a function of three-body mass would probably be consistent when compared with the results of a more complete formalism. One should be quite careful, on the other hand, of drawing conclusions from comparatively small phase effects since these could be significantly altered by inclusion of sub-energy dependences.

4. Mechanics of the Likelihood Fit

In this and the following chapter, we address the problem of estimation of the partial wave amplitudes $A_{s\eta J}$ from the data. By the nature of this problem, our discussion is generally qualitative and heavily biased to the procedures used in analyzing E-75, E-132 and E-135 data. We shall attempt to record those details of the analysis which were found either essential or practically useful. It should be kept in mind that our procedures are often subjective in nature, although we have attempted to abstract the general methodology out of the mire of our own physics analyses. We have developed several software tools to assist our own analyses, and it will often be convenient to refer to these programs as we proceed. We divide the problem of amplitude estimation into two broad areas: likelihood fits and solution determination. The latter topic is discussed in §5.

The term likelihood fit as discussed in this section will refer to several related problems. In defining a likelihood function we specify certain input requirements for the fitting program. These include such things as data, Monte Carlo information, and first derivatives of the probability distribution. The output of the fitting program includes solutions (the $A_{s\eta J}$) and their error matrix. Provision for managing and storing this information must be made. This chapter will outline the mechanisms by which we have managed these problems.

4.1 OVERVIEW OF THE LIKELIHOOD FITTING

Before turning to the details of the likelihood fitting, it is useful to have an overview of the analysis procedures. This is given by the flow chart in Fig. 10.

The probability that we observe an event (P_{obs}) in the apparatus is the product of the physics probability that it occur (P given in (2.2)) and the probability that it is properly measured in the apparatus ϵ (the acceptance). Traditionally, the acceptance is determined by a Monte Carlo procedure in which events are generated and the effects of the spectrometer are then modeled to determine the acceptance as a function of the kinematical variables describing the event. To properly account for the effect of the data selection procedure on ϵ, the selection cuts placed on the data events must also be applied to the Monte Carlo events in a consistent manner. We choose to do this by putting all the Monte Carlo events through the same selection program used to extract the data event sample. Because of this, our flow chart
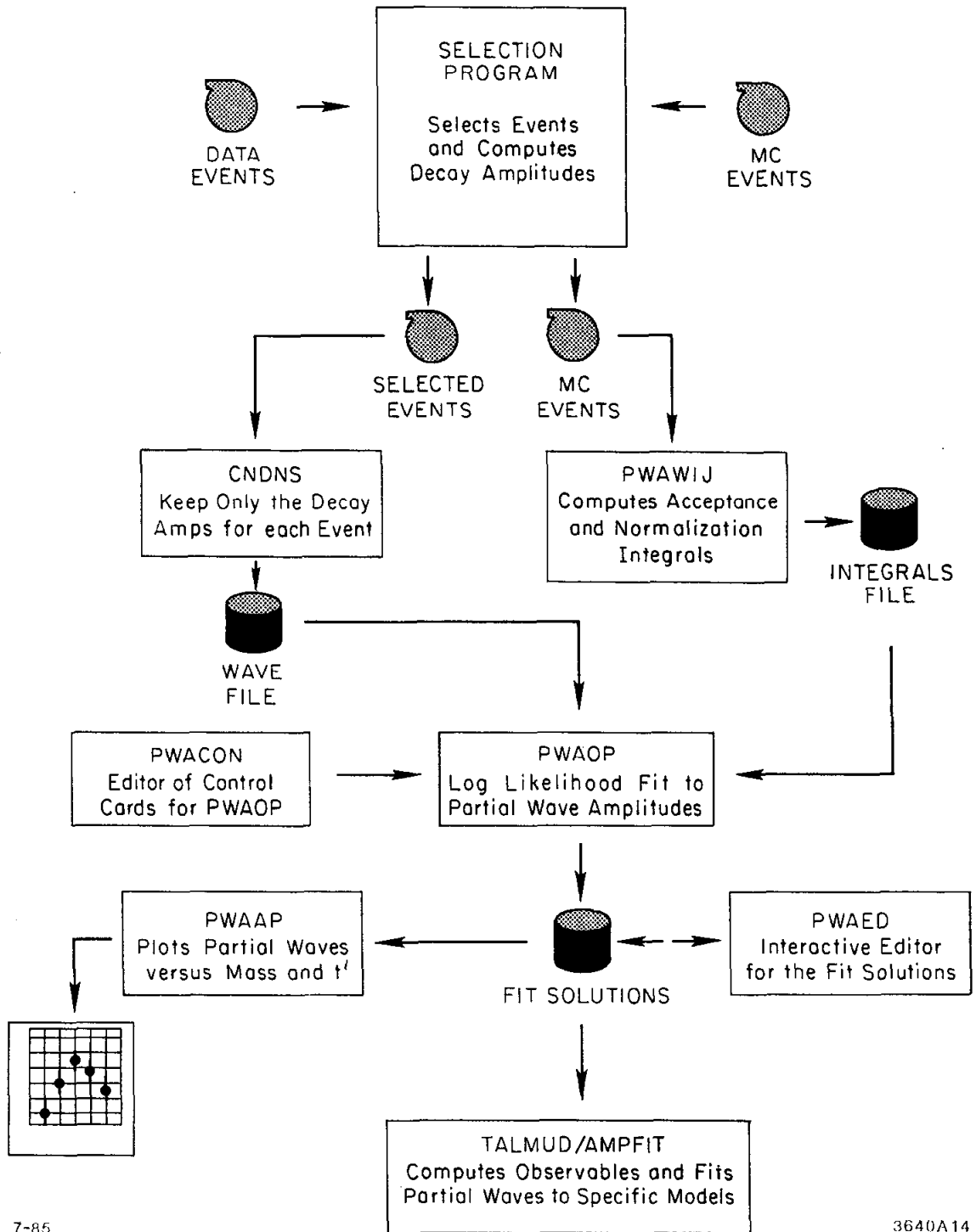
Figure 10. Overview of the three-body analysis

divides into two branches. All of the events (data and Monte Carlo) are required to pass the selection program. For every passed event, the Euler angles describing the three-body final state are computed with a call to the routine **OILER**, and then the routine **CALCPI** is used to compute the decay amplitudes (the $X_{\eta J}$) for the event. The $X_{\eta J}$ from each event are the data needed to perform the likelihood fit. In the case of the Monte Carlo events, besides computing the Euler angles and $X_{\eta J}$ for every event passing the selection using the measured event parameters, the Euler angles and the $X_{\eta J}$ are also computed using the generated event information. This latter information is needed to determine the acceptance corrected partial wave amplitudes.

The $X_{\eta J}$ from the data events then form part of the input into the likelihood fitting program **PWAOP**. The Monte Carlo events are used to compute the other inputs into the fit, namely the acceptance and normalization integrals,

$$W_{\eta I J}^{Acc} = \int \epsilon X_{\eta I} X_{\eta J}^{*} \, d\omega^5 \Big/ \int d\omega^5$$

$$W_{\eta I J}^{Nor} = \int X_{\eta I} X_{\eta J}^{*} \, d\omega^5 \Big/ \int d\omega^5.$$

(4.1)

The integration is done over each mass and t' bin chosen for the analysis by the program **PWAWIJ**. (Strictly speaking, only the $W_{\eta I J}^{Acc}$ are necessary to perform the likelihood fits; the $W_{\eta I J}^{Nor}$, however, are used after the fit to determine the acceptance corrected wave intensities. This will be discussed in more detail in a later section.)

The calculation of the acceptance and normalization integrals predicates a choice of mass and t' binning for the analysis. In principle we would like this binning to be as fine as possible (recall that $A_{s\eta J} = A_{s\eta J}(m, t')$ and those nasty coherence effects). On the other hand our data sample is finite. As a rough estimate we suppose 100 events/wave will determine a complex $A_{s\eta J}$, If we then suspect that perhaps 15 partial waves are important in a given m, t' region, we would introduce an m, t' mesh on our data such that there were ~ 1500 events in each $\Delta m \Delta t'$ box. Having chosen $\Delta m \Delta t'$, we limit our data and the $W_{\eta I J}^{Acc}$, $W_{\eta I J}^{Nor}$ to the region of interest and save the necessary information on disk.

The user drives **PWAOP** by providing it a series of control cards which specify each set of fits. These control cards are normally generated with the aid of **PWA-**

CON, an interactive program which serves as a control card editor. The results of the fitting program **PWAOP** are saved on a number of solution files. This information includes the $A_{s\eta J}$, a subset of the error matrix, and other bookkeeping information. The solutions can be edited using the program **PWAED** and they can plotted, wave-by-wave, using the program **PWAAP**. Both of these activities are necessary to keep track of the solutions as they are churned out by **PWAOP** . We defer a discussion of the "Solution Selection" procedure in Fig. 10 until the next chapter; this decision loop is properly a part of the solution determination procedure.

We now come to the final steps, roughly speaking, in our overview. The program **TALMUD** is designed to study all possible observables (3.16–3.19) as a function of m or t'. As such it is a highly flexible program requiring access to the full error matrices from the fit. Additional inputs to **TALMUD** are the solutions and the $W_{\eta I J}^{Nor}$; the latter are used to correct the final results for the spectrometer acceptance and selection cuts. Most physics conclusions about the partial wave analysis are made on the basis of **TALMUD** output.

Another program **AMPFIT** is designed to accept as input the solutions and the corresponding error matrices and to fit the behaviour of the amplitudes as a function of m and t' to any number of multi-parameter models. For example, we may want to fit the $2^+0^-K^*D$, $2^+1^+K^*D$ and $2^+1^-K^*D$ amplitudes to a common Breit-Wigner amplitude with separate background terms in each wave. **AMPFIT** can fit these three amplitudes simultaneously to that model, taking into account the correlations between these partial wave amplitudes through the error matrices provided by **PWAOP**.

Lastly we may compare the results of the fits with the data using the program **PWACF**. This routine will compare the predicted data distributions derived from the likelihood fit with the observed data distributions, and will also show the effect of the acceptance correction on the various distributions.

This overview of Fig. 10 has been presented as a guide for the codes and methods developed in our $K\pi\pi$ studies. It is not meant as a rigorous guide on how to proceed but it is indicative, rather, of how one might approach the analysis.

4.2 THE EXTENDED MAXIMUM LIKELIHOOD FUNCTION

We assume that the probability for the *ith* event in our sample is given by

$$P_{obs}^{(i)} = P^{(i)}\epsilon^{(i)}, \tag{4.2}$$

where $P^{(i)}$ is the theoretical probability (2.2) for the *ith* event to occur, and $\epsilon^{(i)}$ is the probability that it is observed in the spectrometer and passes the selection criteria. Notice that an event is specified by a unique set of kinematical variables in the sense of (2.5). One may think of $\epsilon^{(i)}$ as being either zero or one depending on the geometry of the apparatus multiplied by an overall weight (≤ 1) reflecting such things as track decay, absorption, tracking efficiency, etc. As we shall see shortly, the $\epsilon^{(i)}$ need *not* in practice be determined for the observed data.

Consider a sample of N observed events in a bin of area $\Delta m \Delta t'$. The likelihood function may be written [25,26]

$$\mathcal{L} = e^{-\overline{N}} \prod_{i=1}^{N} P_{obs}^{(i)}, \tag{4.3}$$

where

$$\overline{N} \equiv \int P_{obs}(\omega)d\omega^5. \tag{4.4}$$

The integral in (4.4) extends over all phase space. Equations (4.3) and (4.4) are functions of the $A_{s\eta J}$. The principle of extended maximum likelihood maintains that the best estimate of the $A_{s\eta J}$ is that which maximizes $\mathcal{L}$.

In practice we work with $\ln \mathcal{L}$. Some interesting simplifications of (4.3) then occur. Using (4.2) and (2.2) we find

$$\ln \mathcal{L} = \sum_{i=1}^{N} \ln \epsilon^{(i)} + \sum_{i=1}^{N} \ln P^{(i)}$$
$$- \sum_{s\eta} \sum_{I} \sum_{J} A_{s\eta J} A_{s\eta J}^{*} \int \epsilon(\omega) X_{\eta J}(\omega) X_{\eta J}^{*}(\omega) d\omega^5. \tag{4.5}$$

We note that the acceptance for the observed events may be effectively dropped from (4.5). This follows since the first term is an overall scale to $\ln \mathcal{L}$ which is independent of the value of the amplitudes and the number of waves; so long as we

consider the same bin, it is constant. The other important simplification is seen in the third term of (4.5). Acceptance only enters through the acceptance integrals which may be computed independently of the actual values of the amplitudes.

Our likelihood function thus reduced to

$$\ln \mathcal{L} = \sum_{i=1}^{N} \ln P^{(i)} - \sum s\eta \sum_I \sum_J A_{s\eta I} A_{s\eta J}^* W_{\eta I J}^{Acc} \qquad (4.6)$$

where

$$W_{\eta I J}^{Acc} = \frac{1}{N_t} \sum_{i=1}^{N_t} \epsilon^{(i)} X_{\eta I}(\omega_i) X_{\eta J}^*(\omega_i). \qquad (4.7)$$

Equation (4.7) is the Monte Carlo evaluation of the acceptance integral defined in (4.1); N_t is the number of thrown events in the particular mass and t' bin. The sum in (4.7) is effectively only over the Monte Carlo events which are detected in the apparatus and satisfy the selection cuts, since $\epsilon^{(i)}$ is zero otherwise. The second term in (4.6) is the number of observed events $\overline{N}$ predicted by the fit. In principle, and in practice for good fits, this integral is quite close to the number of observed events N. At the end of each fit, **PWAOP** scales the parameters $A_{s\eta J}$ to ensure that this is so.

For N large ($\sim 10^3$), we can roughly estimate the scale on $\ln \mathcal{L}$. At the end of fit

$$\ln \mathcal{L} \sim \sum_{i=1}^{N} \ln P^{(i)} - N$$

The average value of $P^{(i)}$ is roughly $N/\langle \epsilon \rangle$ where $\langle \epsilon \rangle$ is some average acceptance. We thus estimate

$$\langle \ln \mathcal{L} \rangle \sim N \ln \left(\frac{N}{\langle \epsilon \rangle} \right) - N. \qquad (4.8)$$

For E-75 with $\langle \epsilon \rangle \sim 12\%$ and $N \sim 10^3$, (4.8) gives $\ln \mathcal{L} \simeq 8N$ which is what was observed.

4.3   SOME DETAILS ON THE INPUT TO THE FIT

As mentioned earlier, the user of **PWAOP** is responsible for inputs of data and acceptance and normalization integrals. The fitting program uses a multi-purpose fitting algorithm called **OPTIME**[27] which performs the actual $\ln \mathcal{L}$ maximization.

OPTIME employs subroutine **HUME** that computes such quantities as P and its derivatives with respect to the fit parameters $A_{s\eta J}$. As this information would be needed for any implementation of this three-body analysis, we record some of the relevant details here.

Consider the probability distribution,

$$P = \sum_{\substack{s=\pm \\ \eta=\pm}} \left| \sum_J A_{s\eta J} X_{\eta J} \right|^2 . \tag{2.2}$$

This is the basic expression computed in **HUME**. Recall that (2.2) assumes no nucleon polarization information. Should a reaction such as $K^- p \to \bar{K}^\circ K^+ \pi^- \Lambda$ be studied, (2.2) and the corresponding acceptance integral (see (4.11) below) would have to be modified. One way of doing this is described by Wagner [28]. After a bit of algebra, the first derivatives of (2.2) are shown to be

$$\frac{\partial P}{\partial Re(A_{s\eta J})} = 2Re \left(\sum_I A_{s\eta I} X_{\eta I} X_{\eta J}^* \right)$$

$$\frac{\partial P}{\partial Im(A_{s\eta J})} = 2Im \left(\sum_I A_{s\eta I} X_{\eta I} X_{\eta J}^* \right) . \tag{4.9}$$

In addition to these derivatives (4.9), we must also provide **OPTIME** with derivatives of the predicted number of observed events $\overline{N}$ defined in (4.4).

$$\frac{\partial \overline{N}}{\partial Re(A_{s\eta J})} = 2Re \left(\sum_I A_{s\eta I} W_{\eta I J}^{Acc} \right)$$

$$\frac{\partial \overline{N}}{\partial Im(A_{s\eta J})} = 2Im \left(\sum_I A_{s\eta I} W_{\eta I J}^{Acc} \right) . \tag{4.10}$$

4.4 COMMENTS ON THE ACCEPTANCE CALCULATION

As we have seen from our formulation of the likelihood function (4.5–4.6), the acceptance of the apparatus appears only in the normalization integrals $W_{\eta I J}^{Acc}$ defined in (4.1). These in turn are calculated by Monte Carlo techniques. It is

therefore essential that the MC program properly incorporate all cuts, acceptances, decay probabilities, detection efficiencies, etc., that could have affected the observed data. In the course of the partial wave analysis, it may be necessary to impose further cuts on the data; such cuts must also be incorporated into the MC data when the $W_{\eta I J}^{Acc}$ are computed. For a high acceptance apparatus, the most likely such cuts will be to remove low mass Δ's, N^*'s and/or Y^*'s. Although the partial wave decomposition of the $K\pi\pi$ system could in principle describe such data, the number of waves required would be prohibitive, especially for prominent Δ or Y^* signals.

Beyond these remarks there are other important considerations which must be addressed before generating the MC events. Among them are:

1. How many MC events?
2. How should they be distributed in m and t'?
3. What *a priori* information should be included in B_J (see §2.5)?
4. Do we compute waves in the s or t channel, or in both?

In what follows we discuss the procedures adopted in our experiments (E-75, E-132 and E-135) to address these issues.

The number of MC events one chooses to generate is closly related to the chosen event distribution in m and t'. These choices follow from considering how the data are distributed and from the need to have reliable estimates of $W_{\eta I J}^{Acc}$ and $W_{\eta I J}^{Nor}$. In Table 1 we show the m and t' distribution of the observed $K^+\pi^+\pi^-$ data events from E-75. The table was arrived at after several iterations, using several criteria. It was realized at an early stage that the $W_{\eta I J}^{Acc}$ should be available in a much finer $\Delta m \Delta t'$ mesh than would ever be used in a fit. This gave us the freedom of not having to fix the binning of the data before we knew the important physics features. The lower limit on Δm was chosen to keep at least some (≥ 20) events in each t' slice. The number of MC events required to pass in each bin, N_p, was chosen to be about 10 times the number of observed events. Note that this requires some *a priori* knowledge of acceptance in each bin so that the number of thrown events, N_t, could be properly chosen. This number of MC events was chosen to keep the error in the evaluation of $W_{\eta I J}^{Acc}$ and $W_{\eta I J}^{Nor}$ small relative to the statistical weight of the data.

Table 1. The Monte Carlo binning used in the E-75 $K^+\pi^+\pi^-$ analysis. The m and t' numbers are leading bin edges. Each m and t' node is the number of observed events in the bin. The last t' bin is from 0.6 to 1.0 $(GeV/c)^2$.

									$m(K^+\pi^+\pi^-)$								
		1.00	1.04	1.08	1.12	1.14	1.16	1.18	1.20	1.22	1.24	1.26	1.28	1.30	1.32	1.34	1.36	1.38
	0.00	107	316	548	286	369	412	449	506	519	514	475	429	385	358	386	358	292
	0.01	110	225	448	291	275	327	373	384	414	434	410	316	346	306	305	286	247
	0.02	74	209	342	231	272	279	339	348	376	395	350	316	308	258	250	238	220
	0.03	67	199	303	185	223	248	272	293	321	354	264	308	263	244	244	209	206
	0.04	83	180	265	176	174	188	237	199	270	254	289	253	214	238	197	211	193
	0.05	55	138	251	146	185	194	189	240	246	268	257	215	200	227	181	182	162
	0.06	53	144	208	135	171	172	164	204	209	228	222	204	175	164	160	145	166
	0.07	39	115	176	120	140	133	178	190	203	174	214	177	136	160	154	147	140
	0.08	64	177	291	217	227	257	284	289	348	314	348	294	284	261	280	255	224
t'	0.10	62	151	223	157	182	207	234	231	282	281	284	252	236	223	192	197	216
	0.12	42	94	201	121	135	167	171	194	211	214	202	195	191	183	199	182	162
	0.14	33	80	126	99	112	122	164	135	175	192	173	165	149	160	132	149	124
	0.16	34	77	123	70	95	112	123	133	148	151	133	123	137	129	116	112	112
	0.18	31	65	81	54	67	85	87	97	127	106	122	116	109	96	110	86	96
	0.20	17	42	77	44	61	69	78	86	88	93	85	87	109	83	88	85	77
	0.22	30	65	121	61	75	110	113	118	170	155	142	120	143	132	116	129	126
	0.26	17	54	67	56	50	80	65	72	97	99	106	81	102	81	103	64	88
	0.30	31	67	97	69	66	83	83	108	93	128	117	112	100	122	126	146	129
	0.40	19	19	35	23	33	23	28	53	47	48	53	66	53	37	48	59	59
	0.50	7	5	21	12	12	13	15	18	16	23	37	28	283	33	34	34	33
	0.60	11	23	26	14	18	27	17	21	42	61	41	39	39	33	39	45	45

Since the data was fit in bins which will in general be larger than the bins for which the $W^{Acc}_{\eta I J}$ are computed in, these integrals were averaged over each data bin when the inputs to the fit were set up. This averaging was done with the following formula

$$\langle W^{Acc}_{\eta I J}\rangle = \frac{\sum\limits_{k}\left(N_0^{(k)}/\langle\epsilon_k\rangle\right)W^{Acc}_{\eta I J}{}^{(k)}}{\sum\limits_{k}\left(N_0^{(k)}/\langle\epsilon_k\rangle\right)} \qquad (4.11)$$

where

$$\langle\epsilon_k\rangle = \frac{1}{N_t}\sum_{i=1}^{N_t}Acc_i, \qquad (4.12)$$

in the notation of (4.7). The index k runs over the bins of Table 1 which were to be averaged, and $N_0^{(k)}$ is the number of observed events in the kth bin. Notice that (4.11) and (4.12) assume that the number of events passed by the Monte Carlo in each bin was in proportion to the observed event distribution in m and t', i.e. $N_t^{(k)}\alpha N_0^{(k)}/\langle\epsilon_k\rangle$. Since $N_0^{(k)}/\langle\epsilon_k\rangle$ is roughly the true number of events in each bin, the averaged normalization integrals, $W^{Nor}_{\eta I J}$, were also computed using (4.11) and (4.12). Even with these qualifications, (4.11) remains an approximation which becomes worse as the number of bins averaged increases.

For each mass slice in Table 1, t' slopes were determined from the observed spectrum. Monte Carlo events were generated in the corresponding t' bins according to these distributions corrected for the t' acceptance of the apparatus. This amounts to assuming that each wave has the same t' dependence; that is

$$B_J \propto f_J(m,t') = e^{\frac{bt'}{2}}, \qquad \text{for all } J. \qquad (4.13)$$

Note, however, that the function $f_J(m,t')$ in (2.9) was set to one for all waves both for the data and the MC events. This would seem to be inconsistent with distributing the MC events as $e^{bt'}$ also. To see that there is no inconsistency, suppose we had computed waves with (4.13) but generated the MC events flat in t'. In this case (4.6) and (4.7) become

$$\ln \mathcal{L} = \sum_i \ln\left\{\sum_{s\eta}\left|\sum_J A_{s\eta J}X_{\eta J}(\omega_i)\right|^2\right\} + \sum_i bt'_i$$

$$-\sum_{\substack{IJ \\ s\eta}} A_{s\eta I} A_{s\eta J}{}^* W_{\eta IJ}^{Acc} \qquad (4.6')$$

where

$$W_{\eta IJ}^{Acc} = \frac{1}{N_t} \sum_{k=1}^{N_t} \epsilon^k e^{bt'_k} X_{\eta I}(\omega_k) X_{\eta J}^*(\omega_k). \qquad (4.7')$$

Notice that $X_{\eta I}$ in $(4.6')$ and $(4.7')$ denotes the decay amplitude with $f_J(m,t') = 1$; that is, with no $e^{bt'/2}$ dependence. We see from $(4.6')$ that a t' dependence which is the same for all waves simply contributes a constant term to lnL. On the other hand, this dependence occurs in $(4.7')$ in a manner equivalent to having generated MC events according to $e^{bt'}$. The advantage of generating the Monte-Carlo events in accordance with the major trends in the data distributions is that the Monte Carlo result for the acceptance is obtained "efficiently," i.e. the acceptance measurement has the most accuracy in the kinematical regions with the largest number of data events.

Although we might expect each wave to have a different t' dependence, we generally do not have sufficient information to specify that dependence before the partial wave analysis. The best we can do is to generate MC events according to the t' distribution observed in each mass slice. The above discussion shows that this is equivalent to having used (4.13) and MC events with a flat t' distribution. Once the partial wave analysis has been done and we know something about the t' dependence of each wave, we should in principle repeat the fits using this information. In practical terms, this requires that both the data and MC waves must be modified and the normalization integrals recomputed. Note, however, that it is not necessary to recompute the $X_{\eta I}$ nor to regenerate MC events.

As a concrete example, suppose that the partial wave analysis indicates a function $f_J(m,t')$ for each wave, and that the MC events have been generated according to $e^{bt'}$. Then the data and MC waves should be modified in the following way:

$$X_{\eta I} \rightarrow \begin{cases} f_J(m,t') X_{\eta I}, & \text{for data events, and} \\ f_J(m,t') X_{\eta I} e^{\frac{-bt'}{2}}, & \text{for MC events.} \end{cases} \qquad (4.14)$$

4.5 ANALYSIS IN THE S-CHANNEL

It may happen that certain results of a partial wave analysis performed in the t'-channel are better emphasized in the s-channel. We record here the formulae

necessary to do this. As in the case of a t'-dependence, we can set up s-channel fits without recomputing the $X_{\eta J}$ or regenerating MC events.

In the rest frame of the $K\pi\pi$ system, we take the s and t-channel z-axes to be

$$
\begin{aligned}
\hat{z}_s &= -\hat{p}_{out} \\
\hat{z}_t &= \hat{K}^+_{in}.
\end{aligned}
\tag{4.15}
$$

The cosine of the angle between $\hat{z}_s$ and $\hat{z}_t$ is given by

$$
\cos\theta_{ts} = \frac{p^2_{K\pi\pi}(p_{K^+_{in}} \cdot p_{p_{out}}) - (p_{K\pi\pi} \cdot p_{K^+_{in}})(p_{K\pi\pi} \cdot p_{p_{out}})}{\sqrt{\Delta_2(p_{K\pi\pi}, p_{K^+_{in}})\Delta_2(p_{K\pi\pi}, p_{p_{out}})}}
\tag{4.16}
$$

where $\Delta_2(a, b) = a^2 b^2 - (a \cdot b)^2$. The dot products in (4.16) are between the 4-vectors $p_{K\pi\pi}$, $p_{K^+_{in}}$ and $p_{p_{out}}$.

In the $|JM\rangle$ basis the desired transformation is

$$
\tilde{G}^{(s)}_{JM} = \sum_{M'} \tilde{G}^{(t)}_{JM'} d^J_{MM'}(\theta_{ts}).
\tag{4.17}
$$

To go to the $|J|M|\eta\rangle$ basis we use (cf. (3.8) and (3.11))

$$
G_{\eta J|M|} = N_M \left(\tilde{G}_{JM} + (-1)^{J+L+l+M} \tilde{G}_{J-M} \right),
\tag{4.18}
$$

where we have denoted the angular part of the decay amplitudes in the t and s-channel by $\tilde{G}^{(t)}_{JM}$ and $\tilde{G}^{(s)}_{JM}$, respectively. We find from (4.17) and (4.18) the result

$$
\begin{aligned}
G^{(s)}_{\eta J|M|} = 2N_M \sum_{M'\geq 0} N_{M'} \\
\left[d^J_{M'|M|}(\theta_{ts}) + \eta(-1)^{J+L+l+M} d^J_{M'-|M|}(\theta_{ts}) \right] G^{(t)}_{\eta J|M|}.
\end{aligned}
\tag{4.19}
$$

Notice that the transformation from the t to the s-channel basis does not mix parity eigenstates. As a practical matter, however, we must have all the $G^{(t)}_{\eta J|M|}$ waves $(0 \leq M \leq J)$ to compute any one $G^{(s)}_{\eta J|M|}$.

It is well known that the transformation which relates the decay amplitudes (4.19) will also relate the density matrices. Schematically, if

$$G^{(t)} = DG^{(s)}, \tag{4.20}$$

then

$$\rho^{(s)} = D^\dagger \rho^{(t)} D. \tag{4.21}$$

To the extent that $\rho^{(t)}$ is measured in very fine m and t' bins we can use (4.21). In practice, however, we find that θ_{ts} is a very rapid function of t' and slowly varying in m. It is thus dangerous to use (4.21) when the fits have been performed over broad t' bins.

4.6 COMPARISON OF FIT RESULTS AND DATA

Although the principal need for the MC events is to calculate the acceptance and normalization integrals (4.1), they are also useful in comparing the results of the fits with the data. This is illustrated in Fig. 11. On the left of the figure are shown histograms for the α, $\cos\beta$ and γ distributions of the data. Superimposed on these are the fit histograms obtained from the passed MC data using the weight $P_{obs}^{(i)} = P^{(i)}\epsilon^{(i)}$ (cf. (4.2)) for the ith MC event. In effect, this gives the observed event distribution predicted by the partial wave amplitudes and the Monte Carlo simulation, and provides a method of comparing the results of the fit with the raw data distributions. The right hand column shows the same distributions corrected for acceptance. These latter histograms were obtained using all the generated MC events weighted by $P^{(i)}$ for the ith event.

Given the large acceptance losses in α and $\cos\beta$, it is worthwhile discussing 1) whether we believe the results, and 2) by what magic do we accomplish such large corrections. Consider the corrected $\alpha\beta\gamma$ distributions; these Euler angles are for the K^* isobar, $K\pi\pi \to K^*\pi$. It is well known that most of the events in this region correspond to $J^P = 1^+$ for the K^* and π in the S-wave. From the $\cos\beta$ plot ($\beta = \cos\theta_{G-J}$) we see an S-P interference with the S-wave dominant. The P-wave corresponds to a bit of the $0^- K^* P$ wave. Turning to the α plot, we see something rather similar to $1 + 4\cos^2\alpha$ which is what is expected for dominant $1^+ 0^+ K^* S$. The γ distribution is flat in accord with approximate t-channel helicity
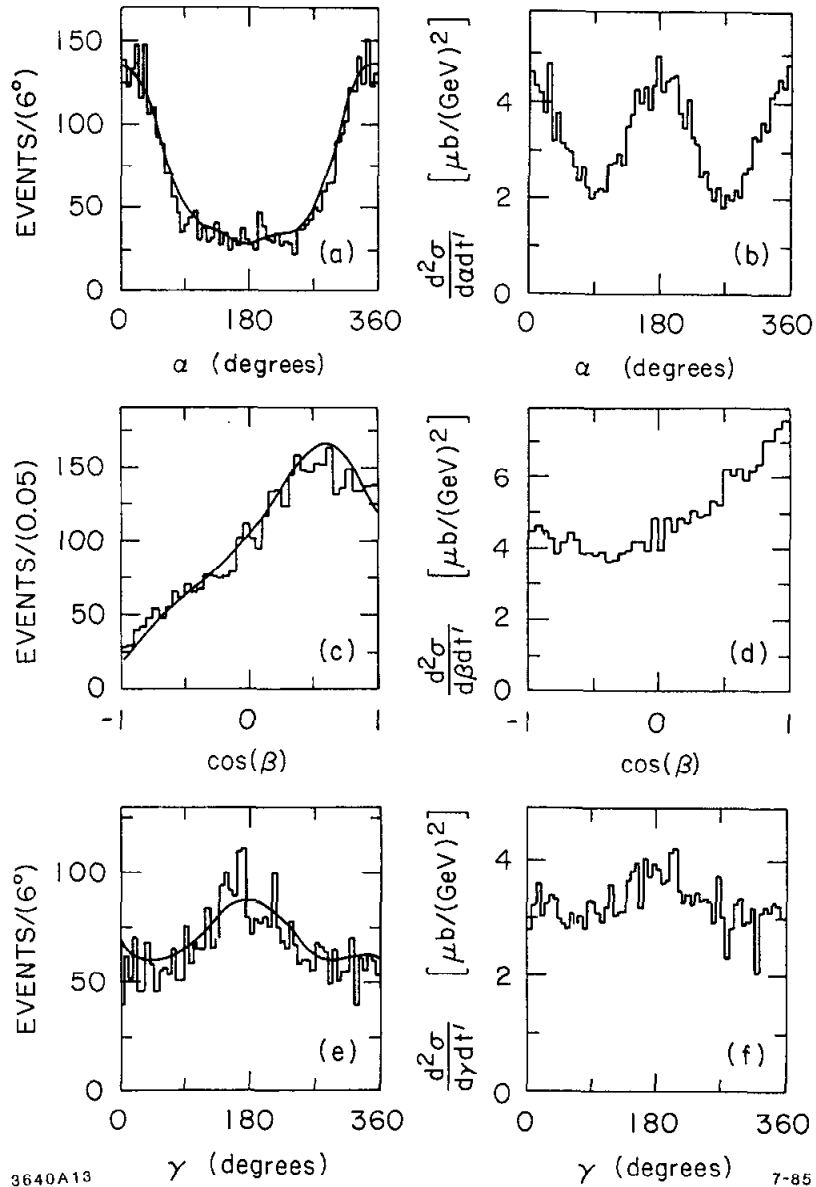
Figure 11. Comparison of a typical fit with data for the K^* isobar. Observed (histograms) and predicted (curves) distributions are on the left, corrected distributions on the right.

conservation. We conclude that these distributions are consistent with what is known about diffractive $K\pi\pi$ production.

Although there are significant losses in the α and β distributions of Fig. 11, there are several good reasons why the analysis could still be performed. First the statistics where acceptance is high are quite good. There are regions in each of the distributions which are only marginally affected. Coupled with these observations is the fact that each decay amplitude has definite symmetry properties in $\alpha\beta\gamma$; thus, for example, losses for $\alpha \sim 180°$ are compensated by symmetry and no losses at $\alpha \sim 0°$. Lastly, we are fortunate that there are few partial waves active in this, the $Q_1(1270)$ and $Q_2(1400)$ region; namely $J^P = 0^-, 1^+$, and 2^+. With respect to the β distribution, for example, we are studying mostly S and P-wave interferences. Had there been 2^- and 3^+ waves present, the analysis may not have been as successful.

4.7 DETAILS ASSOCIATED WITH THE FIT OUTPUT

We conclude this section by describing the contents of a solution record produced by the fit. In addition we record the details of the error propagation in going from amplitudes to the observables (3.16–19), as performed in **TALMUD**.

The results of each fit, a solution, are written to one record of a direct access disk file (see IBM's description of the **DEFINE FILE** statement). The disk file is subdivided into a number of fixed length records, the first record being an index of which records in the file contained valid solutions. **PWAOP** would first read the index, determine the next available empty record on the file, write the new solution onto it and finally update the index record. Besides minimizing the bookkeeping, this allows a number of jobs to be accessing the same file simultaneously. Having three or more fit jobs running on the SLAC computer, each reading and writing the same solution file, is not uncommon.

The information on one solution record consists of:
1. the mass and t' bin being fit;
2. the list of waves used in the fit;
3. the real and imaginary parts of each fitted amplitude;
4. the fit quality, $\ln \mathcal{L}$ and the estimated increase in $\ln \mathcal{L}$ which would have occured in the next step, and
5. the diagonal of the error matrix, and the covariance of the fitted real and

imaginary parts of each wave.

The portion of the error matrix stored on a record is sufficient to be able to determine the acceptance corrected intensity, σ_J, and phase, ϕ_J, of each wave, along with the errors on these two quantities. Let $a_J \simeq Re(A_{s\eta J})$ and $b_J \simeq Im(A_{s\eta J})$. Then σ_J and ϕ_J are related to the fitted amplitudes by the following:

$$\sigma_J = \frac{\sigma_0}{\Delta m \Delta t'}(a_J^2 + b_J^2)W_{\eta JJ}^{Nor}$$

$$\phi_J = \arctan\left(\frac{b_J}{a_J}\right)$$

(4.22)

σ_J then is the differential cross-section for the Jth wave in the fitted mass bin, and ϕ_J is the phase of this wave relative to the partial wave used as a reference wave for that η term (see §5). A short calculation yields the errors on these quantities

$$\sigma_{\sigma_J} = 2\frac{\sigma_0}{\Delta m \Delta t'}W_{\eta JJ}^{Nor}\sqrt{a_J^2 V_{a_J a_J} + 2a_J b_J V_{a_J b_J} + b_J^2 V_{b_J b_J}}$$

$$\sigma_{\phi_J} = \frac{1}{a_J^2 + b_J^2}\sqrt{b_J^2 V_{a_J a_J} - 2a_J b_J V_{a_J b_J} + a_J^2 V_{b_J b_J}}.$$

(4.23)

Note from (4.23) that the errors on σ_J and ϕ_J can be strongly correlated for a given wave; in assessing the statistical significance of a wave we must consider both σ_J and ϕ_J. We can think of the change of variables from $(a_J, b_J) \rightarrow (\sigma_J, \phi_J)$ as a nonlinear transformation, and in that sense (4.23) is a first order mapping of the error ellipse from one set of variables to another. In particular, the mapping into ϕ_J becomes highly non-linear as $\sigma_J \rightarrow 0$, so that σ_{ϕ_J} from (4.23) becomes increasingly unreliable in this limit. Because of this, some caution must be taken when interpreting the phase behaviour of a relatively weak wave; the calculated σ_{ϕ_J} often underestimates the "true" uncertainty in ϕ_J.

The full error matrix from the fit can be written onto a special "error matrix" disk file, for subsequent use by **TALMUD** and **AMPFIT**. The full error matrix is needed when the cross-section and associated uncertainty is computed for any specified set of waves. We present the relevant formulae for such a calculation below, using as an example, the calculation of the error on the total differential

cross section. We begin by rewriting (3.16)

$$\frac{d^2\sigma}{dmdt'} = \frac{\sigma_0}{\Delta m\Delta t'} \sum_{\substack{IJ \\ s\eta}} A_{s\eta J} A_{s\eta J}{}^* W_{\eta IJ}^{Nor}.$$

Expanding real and imaginary parts explicitly as in (4.22-23)

$$\frac{d^2\sigma}{dmdt'} = \frac{\sigma_0}{\Delta m\Delta t'} \sum_{\substack{IJ \\ s\eta}} [a_I a_J + b_I b_J + i(a_J b_I - a_I b_J)] W_{\eta IJ}^{Nor}.$$

Then by the "Word", we can calculate the error

$$\sigma_{\frac{d^2\sigma}{dmdt'}} = \sum_{IJ} \frac{\partial}{\partial a_I} \frac{d^2\sigma}{dmdt'} V_{a_I a_J} \frac{\partial}{\partial a_J} \frac{d^2\sigma}{dmdt'} + 2\sum_{IJ} \frac{\partial}{\partial a_I} \frac{d^2\sigma}{dmdt'} V_{a_I b_J} \frac{\partial}{\partial b_J} \frac{d^2\sigma}{dmdt'}$$
$$+ \sum_{IJ} \frac{\partial}{\partial b_I} \frac{d^2\sigma}{dmdt'} V_{b_I b_J} \frac{\partial}{\partial b_J} \frac{d^2\sigma}{dmdt'}. \qquad (4.24)$$

Computation of the derivatives is not difficult:

$$\frac{\partial}{\partial a_I} \frac{d^2\sigma}{dmdt'} = \frac{\sigma_0}{\Delta m\Delta t'} \sum_{J} \left[\left(a_J W_{\eta JI}^{Nor} + a_J W_{\eta IJ}^{Nor} \right) + i \left(b_J W_{\eta JI}^{Nor} - b_J W_{\eta IJ}^{Nor} \right) \right].$$

But by its definition,

$$W_{\eta IJ}^{Nor} = W_{\eta JI}^{Nor}{}^*,$$

then

$$\frac{\partial}{\partial a_I} \frac{d^2\sigma}{dmdt'} = 2\frac{\sigma_0}{\Delta m\Delta t'} \sum_{J} \left[a_J Re(W_{\eta JI}^{Nor}) - b_J Im(W_{\eta JI}^{Nor}) \right]. \qquad (4.25)$$

Similarly, we find that

$$\frac{\partial}{\partial b_I} \frac{d^2\sigma}{dmdt'} = 2\frac{\sigma_0}{\Delta m\Delta t'} \sum_{J} \left[a_J Im(W_{\eta JI}^{Nor}) + b_J Re(W_{\eta JI}^{Nor}) \right]. \qquad (4.26)$$

Note that the sums in (4.25-26) are over waves of the same η only.

TALMUD also calculates the coherence and relative phase of any two waves, I and J, of the same η. Rewriting then (3.17-18) in terms of the density matrix ρ,

$$\phi_{IJ\eta} = \arctan\left(\frac{Im(\rho_{IJ\eta})}{Re(\rho_{IJ\eta})}\right),$$

and

$$C_{IJ\eta} = \sqrt{\frac{Re(\rho_{IJ\eta})^2 + Im(\rho_{IJ\eta})^2}{\rho_{II\eta}\rho_{JJ\eta}}}$$

where

$$\rho_{II\eta} = \sum_s (a_I^2 + b_I^2) W_{\eta II}^{Nor}$$

$$\rho_{IJ\eta} = \sum_s (a_I + ib_I)(a_J - ib_J)\sqrt{W_{\eta II}^{Nor} W_{\eta JJ}^{Nor}}.$$

The errors are again obtained by propagation in the same way as (4.24).

5. Finding the Solution

Having established the mechanics of describing the data with (2.2), we now discuss how the solutions for the partial waves are obtained. We begin by considering the flow chart for the solution determination procedure shown in Fig. 12.

5.1 OVERVIEW

From the results of the previous analyses or from physics prejudices, one starts by choosing an initial set of partial waves, which we shall call the "base set". The relative magnitude of these waves are established through a process of "random starts". Thus in each mass and t' bin, we perform several (~ 100) likelihood fits where the initial values of the amplitudes are randomly assigned. In general the results of such random starts are unique; redundant solutions are scrubbed from the solution disk.

Having established a base set, one proceeds by adding one wave at a time to the solution. In practice, a series of fits are performed with each new wave, the new wave being initialized randomly. The significance of the wave to the description of the data is judged both by the $\ln \mathcal{L}$ change per mass bin, as well as by the continuity and bin-to-bin significance of the wave amplitude. If the new wave is of little significance ($\leq 2 - 3\sigma$), it is immediately removed from the wave set, and the fit solutions with the wave included are scrubbed from the solution file. Notice that several new waves may be considered in parallel and that one should try each new wave in all bins to establish the continuity or lack thereof of the wave amplitude.

Once several new waves have been found and assuming the list of possible waves has not been exhausted, we define a new base set by repeating the random starts with the augmented set of waves. Although these new random starts rarely reveal anything new, they do establish confidence in the solutions up to this point. Notice that in the flowchart, we are back in the "add wave" loop; in principle we should try all waves remaining in our list, even those previously tested. Because waves can (and do!) interfere, one has to keep in mind that the effect of two new waves on the quality of the solution can be substantially greater than we would expect from examining the effect each wave had individually.

The flowchart of Fig. 12 was drawn under the assumption of spin coherence. After either the wave list or the analyst is exhausted, we next investigate spin
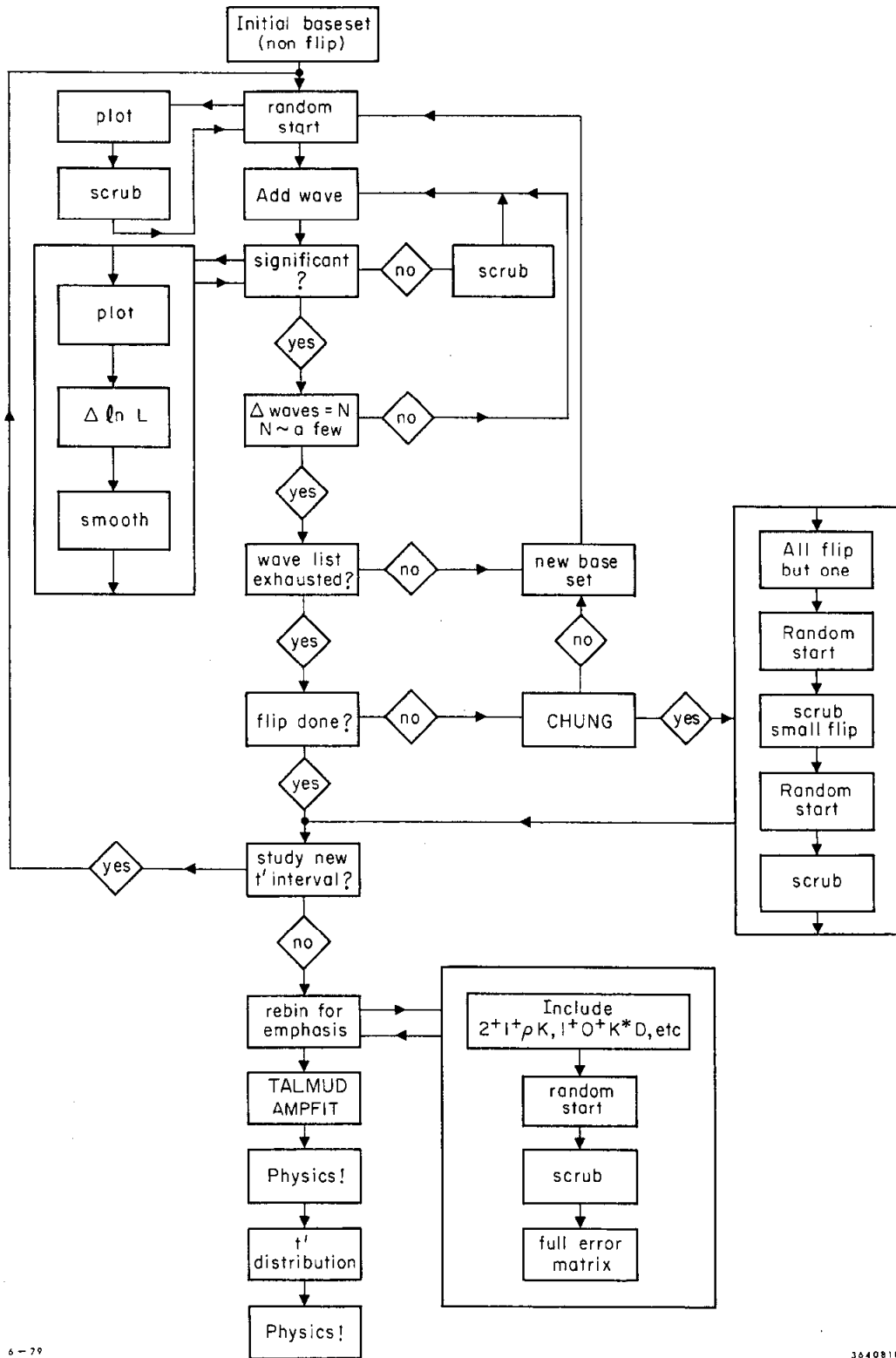
Figure 12. Flow chart for the solution determination procedure

coherence by adding flip waves to the solution. This can be done either with the "add wave" loop or via the "Chung" alternative.

Having established both the non-flip and flip waves, it may be useful to study the data in a different t' interval but still as a function of mass. The flow chart indicates that the "add wave" procedure should in principle again be followed. In practice, one rarely has the energy to do this honestly. Keep in mind, however, that waves of a marginal nature in the previous t' interval may very well be more significant in the new interval. At the very least such waves should be tested. In addition, by changing the t' interval, one tests for spurious coherence effects.

At this point in the analysis, well defined trends will most likely exist in the amplitudes; a physics story may be emerging. It is useful to perform some final fits to emphasize these features by rebinning in mass and using a broader t' interval. In addition, one wants to make quantitative statements about otherwise non-existent waves (e.g. in the $K\pi\pi$ channel, one might wish to determine the ratio of the $1^+0^+K^*S$ and $1^+0^+K^*D$ amplitudes in the Q_1 and Q_2 region). After coming to a final set of amplitudes, the selected fit solutions are refitted with the full error matrix being stored away so that it can be made available to **TALMUD** and/or **AMPFIT**. As remarked earlier, all physics statements should be based on the observables calculated in these programs. Physics features as a function of mass will determine which mass intervals should be used to study the t' dependence of the amplitudes.

Of course a flow chart such as Fig. 12 is at best only a rough guide to establishing a solution. In practice one quite often jumps out of some loop for one reason or another. In this regard, it useful to study initially a small sample of the available data in order to best define the procedure to follow.

In the remainder of this section, we discuss some of the details associated with the various steps indicated in Fig. 12.

5.2 THE INITIAL WAVE SET AND CHOICE OF DATA BINS

The choice of initial waves is a difficult one, as it perforce involves some assumptions about the physics one expects to uncover in the analysis. An obvious first place to start is to review all the available literature on the channel one is studying, and from that source determine which waves one should expect to be significant. It

is a safe bet to include all the low-spin waves in any case, as these have the least impact on the size of the wave set (owing to the fewer magnetic substates). For the higher spin waves, one must try to be realistic and include only those waves which are either known to exist, or are plausible candidates for significant waves.

In practice the problem remains tractable as long as the number of waves in the base set can be kept to a reasonable size. As a concrete example, the E132 $\bar{K}^\circ \pi^+ \pi^-$ analysis had a complete wave set consisting of 142 waves. The base set consisted of only 8 waves, which were drawn from the results of previous analyses of this channel. The final wave set consisted of only 9 waves at low $\bar{K}^\circ \pi^+ \pi^-$ masses and upwards of 16 waves above 1.8 GeV/c^2.

For each set of coherent waves (waves with same nucleon polarization and η), a reference wave must be chosen whose imaginary component is fixed at 0.0 since only relative phases between waves are measurable. This reference wave is normally taken as one of the largest waves in the set, as this is the most stable choice for the given parameterization of the wave amplitudes. This choice has no physics consequences! One is always free to perform an arbitrary rotation of the waves in each incoherent term without changing $\ln \mathcal{L}$.

Since the Monte Carlo data sample is usually generated in the smallest bins with which one can expect to fit the data, the choice of the data bins in which to perform the fits is quite flexible and can be changed relatively easily. The important criteria to consider are that each bin should contain enough events to ensure that the fitted amplitudes are stable from bin to bin, at the same time making the bins small enough so that rapid changes in an amplitude are detectable. Often a suitable compromise is achieved by having a varying bin size which increases as the density of data events decreases, or as the number of fitted waves increases.

It is perhaps appropriate to emphasize a point made earlier. The assumption we have employed throughout is that bin smearing effects are not important. For example, when we calculate the Monte-Carlo acceptance for a bin, the generated events fall inside the bin, but the measured events in general do not. If the acceptance is changing rapidly across the bin, this effect can systematically change the behaviour of the fitted amplitudes (cf. Fig. 8 and the related discussion of coherence effects). There is no generally agreed upon solution to this problem. To the extent

that bin sizes are typically much larger than the smearing of events across bins, this issue is usually not relevant. One, however must be cautious when using bin sizes that approach the resolution of the detector.

5.3 · COMMENTS ON WAVE SELECTION

The process of wave selection is perhaps the most arduous part of the analysis. We have developed a number of software tools which ease this task substantially. Let us describe a typical "add wave" step, as shown in Fig. 12.

The fitting program **PWAOP** uses a stream of input cards to determine the mass bins and waves which should be fitted. A list of possible **PWAOP** input cards is provided in Appendix B. An interactive program **PWACON** is used to set up these cards, although we occasionally take an existing input card file and edit it by hand. Once the **PWAOP** input cards are prepared, the fitting job is submitted to perform the fits.

To examine the fit solutions the interactive program **PWAED** is used to edit the solution files, scrubbing statistically identical solutions and unconverged fits, and sorting the remaining fits in order of likelihood. The interactive program **PWAAP** is then used to plot each wave amplitude (magnitude and phase) as a function of mass or t' for all of the acceptable fit solutions. These plots are then examined by hand to determine the overall significance of the added wave or waves. Once a decision is made, the new solutions are either stored away or scrubbed and another wave is tested.

When a wave is added, the number of parameters used to describe the data increases (i.e. the model becomes more flexible), so in most cases $\ln \mathcal{L}$ of the new solutions will show increases over the solutions using the smaller wave set. We have found that as a rough rule of thumb, a difference in $\ln \mathcal{L}$ of more than 5-10 between two fit solutions in the same bin is significant, especially if the fitted amplitudes are reasonably continuous across neighboring bins. The most powerful criteria we have found is this requirement of continuity across several bins.

The fitted $\ln \mathcal{L}$ function is not necessarily well-behaved, and often has a number of local maxima over the parameter space formed by the partial wave amplitudes. **PWAOP** (and almost every other maximization routine) will converge on one of these local extrema with no guarantee that the maximum found is where $\ln \mathcal{L}$ attains

its global maximum. Which maximum the fit converges to depends strongly on the initial parameters, and so a large number of fits should always be done with the same wave set to the same bin, with a variety of initial parameter values. Unfortunately, there is no practical way of ensuring that the global maximum has been found even after a very large number of fits have been performed with the same model to the same data. Very often **PWAOP** will find the global maximum after a reasonable number of fits have been started. We generally perform 100 fits to each mass bin with the same wave set, and then select the best solutions from each bin. The best solutions in each bin are then used to initialize a fit to the data in the adjacent bins (here **PWACON** comes in very handy). This "propagation" of solutions rarely results in a fit solution which hasn't been seen before. We follow this procedure whenever a new wave set was tried, or when we rebin the data. In addition we find it useful to fit the data in overlapping bins as this gives us more information about the continuity of the solutions as a function of mass. Of course, when it comes down to fitting the partial wave amplitudes to resonances, only amplitudes in non-overlapping bins should be used as only they can be truly considered independent measurements, whereas the amplitudes in overlapping bins are not statistically independent.

5.4   ANALYZING THE FIT SOLUTIONS

Once a final set of waves and solutions have been determined, the most interesting part of the analysis begins, namely understanding the physics which govern the observed behaviour of the partial wave amplitudes. **TALMUD** provides one perspective on the behaviour of the amplitudes. The program computes the physical observables of the model (3.16–3.19) along with the error propagated from the fit error matrices. The behaviour of these observables as a function of mass and t' can then be studied. **AMPFIT** takes a further step and provides the ability to directly fit the various amplitudes to models which either predict their behaviour or the behaviour of the physical observables calculated by **TALMUD**.

The latter approach was used to understand the results of the E132 $\bar{K}^0\pi^+\pi^-$ analysis, and was instrumental in determining the consistency of the measured partial waves with our interpretation of the resonance structure. The E75 data was interpreted with the aid of **TALMUD** alone.

The choice of how one should interpret the behaviour of the partial wave amplitudes is to some extent a matter of taste, as there is no universally accepted model of how a resonant three-body amplitude should behave. In addition to this there is always the question of what behaviour the non-resonant background amplitudes exhibit. One can (and often does!) hypothesize explicit models which predict the behaviour of the amplitudes. To the extent that these models are physically realistic and describe the data, they can be used to answer questions such as what is the mass and width of a resonance decaying through an isobar, how does the resonance's production cross-section fall as a function of t, how coherent the relative production mechanisms are, *etc.*

The fact of the matter is that the model *does* work and produces results which are consistent with our understanding of how resonances form and decay. As long as this is the case and no better description of the data appears on the scene this formalism will continue to be used to describe three-body final states.

Appendix A. Contents of /TRI2/

The kinematic quantities of an event that are relevant to the 3-body PWA are computed by a routine called **OILER**. **OILER** is given the set of 4-vectors which describe each of the initial and final state particles in the laboratory frame, and produces a set of *Euler* angles (cf. §2.2) and invariant masses which can then be used to compute the decay amplitudes for each partial wave.

The quantities computed by **OILER** are listed below in the order that they appear in the **WORD** array which forms the common block **/TRI2/**.

WORD	Variable	Definition
1	m_{123}	the invariant mass of the three meson state
2	t'	4-momentum transfer from beam to 3-meson state
3	m_1	invariant mass of mesons 2 and 3
4	m_2	invariant mass of mesons 3 and 1
5	m_3	invariant mass of mesons 1 and 2
6	θ_1	θ angle for particles 2 and 3
7	θ_2	θ angle for particles 3 and 1
8	θ_3	θ angle for particles 1 and 2
9	α_1	α angle for particles 2 and 3
10	β_1	β angle for particles 2 and 3
11	γ_1	γ angle for particles 2 and 3
12	α_2	α angle for particles 3 and 1
13	β_2	β angle for particles 3 and 1
14	γ_2	γ angle for particles 3 and 1
15	α_3	α angle for particles 1 and 2
16	β_3	β angle for particles 1 and 2
17	γ_3	γ angle for particles 1 and 2
18	mm^2	(missing mass)^2 against 3-meson state

Appendix B. Commands for the PWA Fitting Program PWAOP

PWAOP is the program which performs the maximum likelihood fits to the observed data using the Monte Carlo calculated acceptance integrals. Because of the complexity of the probability function which is used to model the observed event distribution, a typical analysis uses **PWAOP** very heavily, both to develop an understanding of how well the model describes the data and to actually determine the partial wave amplitudes which best represent the observed data distributions. For this reason, a flexible method of driving **PWAOP** exists which allows a user to perform almost any sort of fit.

PWAOP reads a set of input cards which are interpreted as commands to initialize and perform a fit. The entire set of cards can be divided into the specifications for one or more fits. **PWAOP** reads the cards for the first fit, performs the fit, and then commences reading the cards for the next fit.

The information needed to set up a fit can be divided into three categories:

1. The range of mass and t' which specifies the fitted data bin.
2. The partial waves that are to be included in the fit. The reference wave for each incoherent set of waves (i.e. the different η and spin flip/non-flip terms) must also be specified.
3. The initial values of the wave amplitudes. These initial values can come from a solution to a previous fit stored on disk or from the previous fit, or can be defined randomly by **PWAOP** . It is possible to "fix" a subset of the partial waves; they will be considered as constants throughout the fit.

Thus, a fit is specified by defining the data bin, by choosing the waves to be fitted, and by specifying how the waves are to be initialized.

Besides having the ability to define the data bin, a number of special features are available which can be invoked when the data bin is defined. A solution obtained in one mass bin can be propagated across a number of adjacent mass bins in much the same way one fit is specified. One uses a special control card (the "DO LOOP" command) that sets up the first fit in one mass bin, and then intializes the next fit in the adjacent mass bin with the wave amplitudes determined by the first fit. A series of fits in the same mass bin with random initialization of the amplitudes for each fit can be specified with the "RANDOM" command.

There are a number of ways the partial waves can be initialized. Some or all of the wave amplitudes can be initialized randomly, from a previous fit solution, or from values given on the control cards. Any combination of these three methods can be used simultaneously.

The syntax of the **PWAOP** control cards is described below. Each card is an 80 character record; the first column must always contain an asterisk, followed by a keyword that is up to 8 characters long. A blank space is left in column 10, and the rest of the card is divided into 7 8-character fields. For integer arguments, the fields are I8 format, while for floating point arguments the fields are F8.3.

B.1 DEFINITION OF BINS

* BINS   *masslo masshi tlo thi AVERAGE*

This card defines the mass and t' bins for the data. All arguments are floating point. The option AVERAGE specifies that the acceptance integrals are to be averaged across the data bin (if the Monte Carlo binning is finer than the specified data bin).

* DO LOOP   *mbeg mend mstep tlo thi AVERAGE*

This defines a series of fits that propagate a solution from the mass bin $[mbeg, mbeg+mstep]$ through the adjacent mass bins of width *mstep* till the bin with upper or lower limit *mend* is reached. The initialization for the next fit comes from the results of the previous fit in the adjacent mass bin.

* RANDOM   *masslo masshi nfits tlo thi AVERAGE*

This defines *nfits* random starts on the specified mass bin. All the chosen waves are initialized randomly for each fit. All the arguments are floating point.

B.2 SELECTION OF WAVES

* ADD NOFP wv_1 wv_2 wv_3 ...

This adds the waves wv_1 wv_2 wv_3 ... to the set of non-flip waves. The waves are specified by their position in the list of waves. wv_1 wv_2 wv_3 ... is in 7I8 format.

* ADD FLIP wv_1 wv_2 wv_3 ...

This adds the given waves to the flip set of waves.

∗ USE REC   *record unit*

This will add the flip and non-flip waves that were fitted in the fit stored on solution record *record* on the solution disk defined at logical unit *unit*. If *unit* is omitted, it defaults to unit 42.

∗ SCR NOFP wv_1 wv_2 wv_3 ...

This will scrub the specified non-flip waves from the list of fitted waves. Format is 7I8.

∗ SCR FLIP wv_1 wv_2 wv_3 ...

This will scrub the specified flip waves from the list of fitted waves.

∗ FIX NOFP wv_1 wv_2 wv_3 ...

This will fix the specified non-flip waves; they can be initialized to non-zero values, but are not going to be fitted by the program.

∗ FIX FLIP wv_1 wv_2 wv_3 ...

This will fix the specified flip waves.

∗ REF WAV wv_{++} wv_{+-} wv_{-+} wv_{--}

This card defines the reference wave for each incoherent term. The reference waves for the $\eta+$/non-flip and $\eta-$/non-flip are given followed by the $\eta+$/flip and $\eta-$/flip reference waves. Format is 4I8.

B.3 INITIALIZATION OF WAVES

∗ RAN NOFP wv_1 wv_2 wv_3 ...

This causes the specified non-flip waves to be initialized randomly.

∗ RAN FLIP wv_1 wv_2 wv_3 ...

This causes the specified flip waves to be initialized randomly.

∗ INIT REC   *record unit*

This will use the fit solution stored in record number *record* on the solution disk file at logical unit *unit* to initialize the fitted flip and non-flip waves.

∗ INIT ADD   *wave amplitudes*

The floating point values specified in *wave amplitudes* will be used to finish the

initialization of the remaining uninitialized waves. The list of waves is scanned, and whereever a wave is found that has not been initialized, the next two numbers in *wave amplitudes* are used to initialize the wave. Care must be taken so that enough parameters are actually given to complete the initializaition.

* GOFIT

This card signals the end of the cards for the next fit. **PWAOP** will perform the fit as specified, provided that the fit has been initialized correctly. If any cards follow, they will be interpreted as specifications for the next fit.

B.4 EXAMPLES

The first example specifies one fit to be performed on non-flip waves only, with all the waves initialized randomly.

```
*           FIRST ATTEMPT AT KOPI+PI-(N)
*BINS       1.430    1.470   0.000    1.000AVERAGE
*ADD NOFP      2        6      35       85       87      100      102
*REF WAV      35      100       0        0
*RAN NOFP ALL
*GOFIT
```

The next example is the specification of a series of random starts to be performed on one data bin.

```
*RANDOM      1.670    1.710  24.000    0.000    1.000AVERAGE
*ADD NOFP      2        6      35       85       87      100      102
*REF WAV      35      100       0        0
*GOFIT
```

The next set of control lines specifies the propagation of a previously found solution in solution record 38 over a set of adjacent mass bins.

```
*DO LOOP     1.430    1.710    0.040    0.000    1.000AVERAGE
*USE REC       38       41
*REF WAV       35      100       0        0
*INIT REC      38       41
*GOFIT
```

The next example shows how a previouly found solution can be used to partly initialize the fit, and how the rest of the waves can be initialized. Three waves are added to the waves that were fit for the solution in record 2 on unit 42. Two of those waves (111 and 112) are initialized randomly, and the third (109) is initialized as (10.0,10.0).

```
*BINS        1.450    1.490    0.000    1.000AVERAGE
*USE REC        2
*ADD FLIP     109      111      112
*REF WAV       10       60      110      132
*INIT REC       2
*RAN FLIP     111      112
*INIT ADD  10.000   10.000
*GOFIT
```

REFERENCES

1. J.D. Hansen et al., Nucl. Phys. B81, 403 (1974).

2. R.J. Cashmore, "Amplitude Analysis in Three Body Final States" in 14th Scottish Universities Summer School in Physics (1973).

3. G.T. Jones, "Three Meson Partial Wave Analysis–Basic Theory" in Daresbury Study Weekend Series # 8 DL/R34, Feb. 1975 (ed. by J.B. Dainton and A.J.G. Hey).

4. D. Herndon et al., Phys. Rev. D11, 3165 (1975).

5. G. Ascoli et al., Phys. Rev. D8, 3894 (1973).

6. M.E. Rose, "Elementary Theory of Angular Momentum", Wiley, N.Y., 1957.

7. A.D. Martin and T.D. Spearman, "Elementary Particle Theory," North-Holland, Amsterdam, 1970.

8. E. Byckling, "Particle Kinematics," Wiley, N.Y., 1973.

9. R. Levi-Setti and T.A. Lasinski, "Strongly Interacting Particles," U. of Chicago Press, 1973.

10. J.M. Blatt and V.F. Weisskopf, "Theoretical Nuclear Physics," Wiley, N.Y., 1952, p.361.

11. S.U. Chung and T.L. Trueman, Phys. Rev. D11, 633 (1975).

12. G. Cohen-Tannoudji et al., Nuovo Cimento 55A, 412 (1968).

13. G.C. Wick, Ann. Phys. (N.Y.) 18, 65 (1962).

14. R.J. Cashmore, "Sources of Incoherence in 3-Body Partial Wave Analysis" in DL/R34, Feb. 1975.

15. V. Chaloupka, "Some Remarks on Analysis of Multi-Meson Systems" in DL/R34, Feb. 1975.

16. J.D. Hansen, "Evidence for Different Polarization of the $1^+ S K^* \pi$ and $1^+ S K \rho$ Systems" in DL/R34, Feb. 1975.

17. Otter et al., Nucl. Phys. B106, 77 (1976) and private communication.

18. R.J. Cashmore, private communication (1976).

19. I.J.R. Aitchison, "Corrections to the Isobar Model for Three Hadron Final States" in DL/R34, Feb. 1975.

20. J. Werle, "Relativistic Theory of Reactions," North-Holland, Amsterdam, 1966.

21. G. Ascoli and H.W. Wyld, Phys. Rev. D12, 43 (1975).

22. Y. Goradia and T.A. Lasiniski, Phys. Rev. D15, 220 (1977).

23. R.L. Schult and H.W. Wyld, Phys. Rev. D16, 62 (1977).

24. D. Brayshaw, private communication (1976).

25. J. O'Rear, Notes on Statistics for Physicists, Revised, CLNS-82/511, July 1982.

26. G.W. Brandenburg, SLAC Group B Internal Physics Memo # 57 (1974).

27. P.H. Eberhard and W.O. Koellner, Computer Phys. Commun. 3, 296 (1972).

28. F. Wagner, Nucl. Phys. B111, 67 (1976).

2/80